

AD-A284 383



Technical Report 1643
March 1994

Liquid Crystal Tunable Filter

G. L. Adams

Approved for public release; distribution is unlimited.
DTIC Report 1643 DTIC reproduction
SOME MATERIAL IS IN BLACK BOX
REMARKS

DTIC
ELECTE
SEP 16 1994
S B D

94-29991



Approved for public release; distribution is unlimited

DTIC Report 1643 DTIC reproduction

DISCLAIMER NOTICE



THIS DOCUMENT IS BEST QUALITY AVAILABLE. THE COPY FURNISHED TO DTIC CONTAINED A SIGNIFICANT NUMBER OF COLOR PAGES WHICH DO NOT REPRODUCE LEGIBLY ON BLACK AND WHITE MICROFICHE.

Technical Report 1643
March 1994

Liquid Crystal Tunable Filter

G. L. Adams

Electronic Research Laboratory

NAVAL COMMAND, CONTROL AND
OCEAN SURVEILLANCE CENTER
RDT&E DIVISION
San Diego, California 92152-5001

K. E. EVANS, CAPT, USN
Commanding Officer

R. T. SHEARER
Executive Director

ADMINISTRATIVE INFORMATION

Engineers in the Electro-Optic Systems and Technology Branch, Code 843, at the Naval Command, Control and Ocean Surveillance Center (NCCOSC), RDT&E Division, San Diego, CA 92152-5001 conducted this work. Funding for this program was provided by the NCCOSC RDT&E Division, Independent Engineering Development (IED) program under the management of Dr. Kenneth Campbell, Code 014. The program was originally proposed in July 1991 for inclusion in the Fiscal Year 1992 IED budget but was rejected because of funding priorities.

Released by
D. M. Gookin, Head
Electro-Optic Systems
and Technology Branch

Under authority of
C. E. Gibbens, Head
Satellite Communications
Division

Accession For
RTIS GRA&I
DTIC TAB
Unannounced
Justification

By
Distribution Code
Availability Codes
Availability Codes
Special

Dist
A-1

PS

EXECUTIVE SUMMARY

OBJECTIVE

The objective was to manufacture and test a tunable birefringent filter made using liquid crystal variable phase plates. In FY 92, a six-stage tunable birefringent filter was purchased from Meadowlark Optical, Inc. of Longmont, CO. The filter design is a variation on the well-known Lyot-Solc birefringent filter design. The filter was tested using resources available in Code 843 Receiver Laboratory.

RESULTS

Preliminary analysis indicated that the liquid crystal variable phase plates operated as expected and did not seem to degrade the filter performance appreciably. The filter stages were characterized individually and assembled into a composite filter. Testing measured the filter's performance and agreement with theory including characterization of the bandpass, field of view, peak transmission, out-of-band rejection, and transmission uniformity. In general, the measured filter performance agreed with predicted performance and resulted in a filter that was tunable over the specified range with a bandwidth that varied from 1.5 to 3 nm.

RECOMMENDATION

The results of this project were both encouraging and disappointing. A tunable filter was produced with a nominal 2-nm bandpass that tuned anywhere in the blue-green. Unfortunately, the overall peak transmission, out-of-band rejection, and temperature stability of the filter were poor.

Though these problems limited the utility of this device, they are not unsolvable. Meadowlark has already addressed the temperature stability problem in a revised design.

The out-of-band rejection problems can be traced to slight variations between the required retardance of the liquid crystal cells and the actual retardances. These problems could be substantially reduced by carefully recalibrating the cells to ensure that the proper voltage is provided to produce the desired retardance.

The peak transmission problem is not unique to this device, but is inherent in the Lyot design, with its multiple crossed polarizers. This difficulty can be overcome by the use of the Solc design. This design had been rejected in the past because of cost, but the use of inexpensive polymers, or liquid crystal cells as birefringent elements might keep costs manageable.

CONTENTS

INTRODUCTION	1
BACKGROUND	1
THEORY OF OPERATION	3
PHYSICAL DESCRIPTION OF THE FILTER	5
ELEMENTS CONSTRUCTION	7
ELEMENTS	7
Element #1 (Figure 3)	7
Element #2 (Figure 4)	7
Element #3 (Figure 5)	7
Element #4 (Figure 6)	7
Element #5 (Figure 7)	7
Element #6 (Figure 8)	8
PERFORMANCE	8
TEMPERATURE STABILITY	16
CONCLUSIONS	17
PERFORMANCE IMPROVEMENT/FUTURE WORK	17
REFERENCES	19
APPENDICES	
A. MEADOWLARK MODEL	A-1
B. EQUIPMENT LIST AND PROCEDURES	B-1
C. PEAK WAVELENGTH VS VOLTAGE DATA PROVIDED BY MEADOWLARK	C-1
D. PEAK WAVELENGTH VS VOLTAGE DATA PROVIDED BY NRaD FOR ELEMENT #2	D-1
E. FILTER RELIABILITY AND REPAIRS	E-1

FIGURES

1. Polarization forms as a function of phase angle (ϕ)	21
2. Transmission for Lyot filter	22
3. Filter element #1	23
4. Filter element #2	23
5. Filter element #3	24
6. Filter element #4	24
7. Filter element #5	25
8. Filter element #6	25
9. Peak filter transmission vs wavelength, and various contributions to the filter transmission	26

10. Polarizer performance	27
11. Indium tin oxide (ITO) coating transmission	28
12. Filter bandpass, measured and modeled data	29
13. Filter transmission spectrum, filter set at 420 nm	30
14. Filter transmission spectrum, filter set at 490 nm	31
15. Filter transmission spectrum, filter set at 560 nm	32
16. Single element transmission, measured and modeled, element #1	33
17. Single element transmission, measured and modeled, element #2	34
18. Single element transmission, measured and modeled, element #3	35
19. Single element transmission, measured and modeled, element #4	36
20. Single element transmission, measured and modeled, element #5	37
21. Single element transmission, measured and modeled, element #6	38
22. Field-of-view angle, defining geometry	39
23. Transmission vs wavelength and incident angle (3-dimensional plot)	41
24. Transmission vs wavelength and incident angle (contour plot $400 < \lambda < 460$)	43
25. Transmission vs wavelength and incident angle (contour plot $460 < \lambda < 520$)	45
26. Transmission vs wavelength and incident angle (contour plot $520 < \lambda < 600$)	47
27. Transmission vs wavelength and incident angle (50% transmission contour)	49
28. Normalized transmission uniformity contour plot	51
29. Transmission vs wavelength as temperature varies (filter set at 490 nm)	53

INTRODUCTION

BACKGROUND

The Navy has a long standing interest in technology development of blue-green laser systems for various underwater applications. These applications have included communications, non-acoustical antisubmarine warfare, mine detection, and underwater imaging. Recent interest in improving the covertness of these systems by reducing the probability of intercept has resulted in the Navy sponsoring programs to develop frequency agile laser transmitters and receiver systems. Because of the severe background conditions inherent in most applications where these systems would be used, a tunable narrow-band optical filter would be required.

One of the most common technologies for narrow-band optical filters uses birefringent materials to develop a polarization interference filter. These birefringent filters, first proposed in the early 1940s, have been used for years to make narrow-band optical filters with a fixed center frequency. NRaDs* predecessor organization, Naval Ocean Systems Center (NOSC), provided technical direction and guidance for the development of state of the art, large area (1/2 square meter), receiver systems using birefringent filters in the early 1980s. These receiver systems were successfully fielded in the 1984 SLCAIR experiments.

The theory of a tunable birefringent filter is also well developed¹. There are a number of ways to make a birefringent filter tunable. One way is to change the physical thickness of the birefringent material in the optical path. Another method is to place a quarter-wave plate after the birefringent element, and follow it with a rotating half-wave plate in front of the exit polarizer. As an alternative to the rotating half-wave plate, one can use a device with an electrically tunable variable retardation.

In the late 70s tunable filters were designed and manufactured using rotated wave plates. These filters were generally large, bulky, slow, and unreliable because of their mechanical tuning. Until recently the electrically tunable units were not considered practical due to lack of suitable materials. This limitation has been lifted with the advent of commercially available liquid crystal variable phase retarders. These devices have been developed and are manufactured by various companies including Meadowlark Optics, Inc.

The proposal for this program called for the manufacture and testing of a tunable birefringent filter made using these liquid crystal variable phase plates. The filter specifications included an optical bandpass of 2 nm, tunable over the blue-green spectral region from 420 nm to 560 nm.

*NRaD (Naval Command, Control and Ocean Surveillance Center (NCCOSC), RDT&E Division)

THEORY OF OPERATION

The basic birefringent filter is a polarization interference device.¹ At a minimum, it would consist of two polarizers and a piece of birefringent material. In general, birefringent filters are made from a number of these basic elements. The actual design of these types of filters has been well documented in the literature with various overview articles.² The most common designs for birefringent filters are the Lyot-Ohman³ and the Solc.⁴ The design used for this tunable filter is a variation on the Lyot-Ohman filter.

A birefringent material has either two (uniaxial) or three (biaxial) distinct indices of refraction for propagation along different directions in the material. The basic birefringent filter cell only requires two distinct indices (uniaxial material), and in certain geometries for improving the field of view of the filter, biaxial materials are undesirable⁴.

In the Lyot design, the birefringent material is sandwiched between the two polarizers. It is traditional, though not necessary, to arrange the polarizer axes to be either parallel or crossed. The birefringent material is oriented so the axis of the first polarizer is not along one of the principal axes of the material. The usual orientation is at 45 degrees to the principal, or fast axes. When the material is oriented in this manner, the input polarization can be decomposed into two orthogonal polarization components, one along each of the principal axes of the crystal.

Since the index of refraction is different for polarizations along each principal axis, the propagation speed is also different. Because of this difference in propagation velocities, the two orthogonal polarization components become out of phase with each other. As the component propagating along the slow axis becomes progressively more delayed with respect to the fast component, the resulting vector addition of these two components changes. They may no longer form a linear polarization vector, but generally add to form an elliptical polarization vector. The exact form the resulting polarization vector takes is a function of the amount of phase delay experienced by the component propagating along the slow axis. This phase delay (ϕ) can be expressed as

$$\phi = \frac{2\pi(n_e - n_o)d}{\lambda} \quad (1)$$

where d is the path length through the material, n_e is the extraordinary index of refraction, n_o is the ordinary index, $(n_e - n_o)$ is the birefringence of the material (often given the symbol Δn), and λ is the wavelength. When this phase delay is zero, or any multiple of 2π , the resulting polarization is identical to the original. As the phase delay accumulates, the resulting vector goes through a cyclic change from linear to elliptical with the major axis along the original polarization direction, to circular, to elliptical with the major axis along the direction orthogonal to the original direction, back to linear, but orthogonal to the original direction, then back to elliptical, circular, elliptical, all with the opposite sense of rotation to the earlier forms, and finally back to linear with the axis in the original direction (see figure 1).

This changing polarization can be used to create a filter by placing the second polarizer either parallel (maximum transmission when $\phi = 0, 2\pi, 4\pi \dots$), or perpendicular (maximum transmission when $\phi = \pi, 3\pi, 5\pi \dots$) to the first. To design for a particular wavelength between crossed polarizers, the material thickness is chosen to give a phase shift of exactly 2π (or a

multiple) for the wavelength of interest. Because the phase delay is a function of wavelength as well as material thickness (equation 1), the phase delay will be different for every other wavelength. In addition, the situation is complicated by the fact the birefringence of most materials is not constant with wavelength. If this "dispersion of the birefringence" is significant, it must be accounted for. Models describing the effects of this dispersion have been published¹². The net results of these effects is a transmission function that is sinusoidal, with theoretically perfect extinction for wavelength where the phase delay is an odd multiple of π , and unity transmission for wavelength where the phase delay is an even multiple of π . Because of the cyclic nature of the phase shift, oscillating between zero and one, the structure of the filter bandpass goes as the cosine squared of the phase shift⁴. If dispersion is ignored, the transmission is given by

$$T = \frac{1}{2} T_p \cos^2(\phi) \quad (2)$$

where T_p is the transmission of the polarizers.

Lyot-type birefringent filters take advantage of the periodic nature of the bandpass. By stacking a number of cells together and doubling the thickness of each successive cell, the frequency of the pass bands increase by a factor of two as well. When these elements are stacked, the thickest element will determine the spectral bandwidth of the filter, while the thinnest element will determine the free spectral range, or width between successive peaks (figure 2). The tested filter was designed to have six elements, with a bandwidth of 2.2 nm and a free spectral range of 70 nm at 490 nm.

The standard Lyot-type birefringent filter is designed for a specific wavelength, and is, in general, not tunable. The filter can be made tunable by adding a birefringent element that has a variable retardance. In the past, this had been done with mechanically variable devices that actually changed the amount of birefringent material in the beam path.⁵ These devices, though effective, were bulky and susceptible to mechanical failure. In the device under test, Meadowlark has incorporated liquid crystal variable phase retarders.⁶ These are active devices whose birefringence can be controlled by a variable drive voltage. The devices used in this design are driven with a 2-kHz square wave. The amplitude of the driving wave determines the phase delay between the fast and slow axis by changing the birefringence of the liquid crystal material.

PHYSICAL DESCRIPTION OF THE FILTER

The tunable filter includes the following hardware:

- One IBM PC-XT compatible driver board

- Six optical elements

- Seven electrical cables

along with

- Filter driver software

- Filter operations manual

The tunable filter is comprised of six disk-shaped optical elements and a front aperture plate. Each element is 1.5 inches in diameter with a 0.8-inch-diameter optical aperture. The elements' thickness varies depending on their contents (see below). A small flat has been machined as a chord on each element and drilled with a 8-32 tapped hole for mounting to a standard optical post. In addition, each element has four tapped holes through the flat face for connecting to the adjacent element, and two alignment holes and pins to properly align the element. When the six elements are assembled, the filter forms a cylinder 1.5 inches in diameter and 2.85 inches in length. In addition, each element has been fitted with a small (0.25 inch by 0.5 inch) block that holds the electrical connectors. These E. F. Johnson-brand connectors provide the liquid crystal cell drive voltages, which are delivered by RG-174 coaxial cable from the computer controller. Element #6 also contains a connector for an integrated circuit-type temperature sensor that is buried inside the element. This connector was replaced during filter testing and is now a standard 2.5 mm stereo phonograph jack.

Each element consists of various birefringent materials with fixed phase retardance and at least one liquid crystal cell with an electronically variable phase delay for tuning. The overall retardance of the various birefringent materials, and the liquid crystal variable retarder, determines the transmission characteristics of that element. The materials in these elements are sandwiched between a pair of glass-mounted dichroic sheet polarizers (Polaroid Corp. HN42HE). All the elements, except #1, were designed so the input polarizer is a separate piece. Element #1 is designed with two fixed crossed polarizers (see description below). Elements #2 through #6 are designed to operate with parallel polarizers. When the elements are assembled into a composite filter, the output polarizer of element N becomes the input polarizer for element N+1.

The birefringent materials used in these elements include crystalline quartz (elements #5 and #6), three different birefringent polymers, and a liquid crystal cell with fixed retardance (element #3). The three polymers are designated P2, Z1, and T4 by Meadowlark Optics. These designations are pseudonyms for commercially available plastics that have been specifically prepared for this application. Meadowlark has invested considerable time and money in characterizing these materials, and since this data is not commercially available, the actual identities of the polymers are company proprietary and are not included in this report.

The data in appendix C shows there are two fundamentally different constructions/modes of operation for the retardance elements in this filter. In the general case of a liquid crystal variable phase plate, the retardance of the plate drops as the voltage is increased⁷. Appendix C also

illustrates this to be the operational mode of the first three elements. In addition, the voltage vs center wavelength curves for these elements (figures C-1 through C-3) are continuous, indicating a single peak is chased across the entire tuning range of the filter. (This was done to take advantage of the dispersion of the various birefringent elements.) However, in elements #4 through #6, the voltage increases as the filter is tuned from the red to the blue, and the curves jump periodically.

The two effects are related. The rising voltage, as the filter tunes from blue to red, indicates the retardance of the liquid crystal phase plate is increasing, but the overall retardance of the element must decrease to tune from blue to red. This overall decrease is achieved because the variable retarder is placed with its fast axis rotated 90 degrees with respect to the fast axis of the fixed retarder elements. In this way, the increasing retardance of the liquid crystal phase plate is being subtracted from the retardance of the other elements. The larger the retardance of the variable phase plate, the smaller the overall retardance of the element. The variable phase plate is, in effect, speeding up the wave that was slowed in the fixed retarders to achieve the proper overall phase relationship between the two waves. The reason for constructing the element in this way is related to the field of view. The amount of retardance the wave experiences is proportional to its path length through the retarding material. In the thicker elements of the filter, the path length for rays off axis can be significantly longer than the path length for the rays that are on axis. This results in a change in the wavelength of the passed rays that are off axis. To combat this effect, the wide-field designs were developed⁵ In this design, the element is split in half, and the material rotated through 90 degrees to bring the fast axis of the second half of the material into opposition with the fast axis of the first half. When a half-wave plate is included in the center of the element (its effect is to reverse the direction of the fast and slow axis), the operation of the element is unaffected. The polarization plane is rotated in the first half of the element, then reversed in the half-wave plate, and rotated back to its original state. For rays on axis, the effect is negligible; however, for the rays that are off axis, the retardance is reversed and the wavelength distortions that were caused by the longer path length are exactly reversed.

The other characteristic mentioned above is the periodic jumping of the voltage vs center wavelength curve for the three thicker elements. The explanation for this is found in the periodic nature of the pass band of each element. The requirement for maximum transmission at any wavelength is simply for each element to have a peak at the desired wavelength. In the Lyot design, each successive element should have twice as many peaks as the element before it. If it takes a voltage of A volts to tune the single peak in element #1 across the entire tuning range, then it will take a voltage of $A/2$ to tune the two peaks of element #2 across the same range; when there is no voltage on the element, there is already a peak at half the tuning range. As the voltage rises from zero to $A/2$, peak number 1 tunes from the beginning of the tuning range to the middle. If the voltage continues to rise, that peak would continue to tune all the way across the range (as is done in the first three elements of this filter). However, if the voltage is dropped to zero, the second peak will now be in the center of the tuning range, and as the voltage again rises from zero to $A/2$, the second peak will tune from the center of the range to the end. This is the method that has been employed in the last three elements of this filter. The advantage of tuning in this manner is it keeps the voltage levels much lower than would be required if a single peak were driven all the way across the tuning range. The disadvantage is it does not allow the complete exploitation of the dispersion characteristics of the materials being used.

ELEMENTS CONSTRUCTION

ELEMENTS

Element #1 (Figure 3)

This element has both polarizers permanently attached in a crossed configuration. The basic phase retardation (340 nm) is provided by a sheet of T4 polymer. The tuning is accomplished with a single liquid crystal variable retarder, filled with ZLI-2240-100 liquid crystal, designed to have a retardance of 1300 nm. Each side of the liquid crystal cell is coated with a 0.1-mm-thick indium-tin oxide (ITO) coating that is used as a transparent electrode to drive the liquid crystal cell. Both polarizers and the T4 polymer are bound to 0.030-inch-thick glass plates for mechanical stability. The plates holding the polarizers have a broadband antireflection coating on the sides facing out of the element. This element determines the free spectral range of the filter, which is designed to be plus or minus 70 nm at 490 nm, and has a physical thickness of 0.330 inch.

Element #2 (Figure 4)

This stage has a single glass-mounted sheet of T4 polymer (retardance 670 nm) and two liquid crystal variable retarders. The liquid crystal used in these cells is ZLI-2244-100. Each liquid crystal cell has a retardance of 1300 nm. There is only one polarizer permanently attached to this element. The second polarizer can be mounted on the front of the element for testing this stage independent of any other elements. This removable polarizer is mounted between two 0.030-inch-glass plates. Both sides of the detachable polarizer and the outer surfaces of the element have been given a broadband antireflection coating. This element has a physical thickness of 0.485 inch.

Element #3 (Figure 5)

This stage has a single sheet of T4 polymer with a retardance of 1365 nm and three liquid crystal cells (ZLI-2244-100). Two of these cells are variable retarders, while the third is being used as a fixed birefringent element and has a retardance of 1270 nm. As with element #2, the front polarizer is detachable, and all outer surfaces have a broadband antireflection coating. This element is 0.485 inch thick.

Element #4 (Figure 6)

This element uses three different polymers as the basic birefringent element, and a single liquid crystal variable retarder for tuning. The three polymers, T4 (145-nm retardance), Z1 (800-nm retardance), and F2 (7400-nm retardance) are all mounted together between two pieces of optical glass. The liquid crystal cell is filled with ZLI-2140-100. The liquid crystal variable retarder is mounted with its fast axis rotated 90 degrees with respect to the polymers so its retardance counteracts (or subtracts from) the polymers. This change in orientation is used to compensate for dispersion (changing birefringence with wavelength) in the polymers and liquid crystal materials. All outer surfaces have a broadband antireflection coating. This element is 0.375 inch thick.

Element #5 (Figure 7)

This element used quartz as the birefringent material in a traditional wide-field configuration². The quartz is split into two equal pieces with the direction of the optic axis reversed. The

quartz plates are each 1.12 mm thick. An achromatic half-wave plate is placed between the quartz plates, and is made from a piece of Z1 polymer mounted between 0.030-inch-glass plates. Tuning is done with a single liquid crystal cell filled with ZL-2140-100 having a retardance of 1040 nm. Here again the fast axis of the liquid crystal cell is rotated 90 degrees with respect to the half-wave plate to compensate for dispersion. All outer surfaces have a broadband antireflection coating, and the element is 0.40 inch thick.

Element #6 (Figure 8)

This element is essentially identical to element #5 except there are four quartz plates, effectively doubling the birefringent material, and giving twice the retardance. (Four plates were used so all of the quartz pieces would have the same thickness, reducing the production cost.) This element determines the spectral bandwidth of the filter, which is designed to be 2.2 nm at 490 nm. This element is 0.580 inch thick.

PERFORMANCE

The expected performance of the filter was modeled as it was being designed by the engineering staff at Meadowlark (see appendix A). The actual filter performance was measured at NRaD, Code 843. The measurements conducted included measurements of the filter as a whole and the individual elements that make up the filter. The following measurements were conducted between January and October 1993.

1. The peak transmission and filter bandwidth were measured every 5 nm as the filter was tuned across its designed tuning range of 420 nm to 560 nm.
2. Transmission was measured in 1-nm increments, from 400 nm to 600 nm, to determine peak and out-of-band transmission. This measurement was performed for the filter peak transmission set at 420 nm, 490 nm, and 560 nm, respectively.
3. Measurements were made of the transmission of each filter element between crossed polarizers, from 400 to 600 nm in 1-nm increments, for comparison to modeled performance.
4. Verification was completed on the voltage vs center wavelength data provided by Meadowlark, and data generated for filter element #2 after it was repaired.
5. The field of view (or transmission as a function of wavelength and incident angle) of the composite filter was measured.
6. Transmission uniformity over the face of the filter was measured.
7. Attempts were made to measure the speed that the filter switched transmission passbands for 418 nm to 532 nm.

Results of these measurements are as follows:

1. Peak Transmission and Bandwidth

For the most part, the measured performance of the filter was quite close to the modeled performance, with one glaring exception. Whereas the model provided by Meadowlark predicts near unity transmission for any wavelength, the actual filter transmission is considerably less than

10%. Figure 9 shows a plot of peak transmission for the filter as the filter pass band was tuned across the range from 420 nm to 560 nm. Though the data is rather noisy, it clearly shows the peak transmission is on the order of 5% to 10% for polarized input light. (A regression line of the measured data has been included on the plot.) The noise in the data is probably due to less than perfect calibration of liquid crystal cell voltage vs center wavelength set point (measurement #4 described below). If each element is not tuned perfectly to give a peak at the wavelength of interest, the overall filter transmission will suffer, and the filter bandwidth may be slightly enlarged.

Plotted on the same graph is data for the expected transmission of six pairs of parallel Polaroid HN42HE polarizers. This data follows the same trend as the filter transmission data, but peaks between 30% and 35% transmission to polarized input. This curve indicates the maximum expected transmission for the filter even if the birefringent elements had a unity transmission at the peak. In addition, there is also a line labeled "Eighteen Layers ITO." These data show the transmission of the ITO coatings used as transparent electrodes on the liquid crystal cells (see figure 11). These two curves have been combined to generate the data plotted as "Total Loss." The significance of each of these curves is explained below.

Figure 10 shows the measured transmission for the Polaroid HN42HE polarizers used, both singly and in a parallel pair, as well as the calculated transmission for six pairs of parallel polarizers (plotted in figure 9).

The difference between the measured transmission and the transmission through the six sets of polarizers (figure 9) must be due to other loss factors in the filter. The two most severe losses are in the ITO transparent electrodes and fresnel reflection losses from some of the constituent parts of the filter that are either not index matched to the pieces next to them, or have less than perfect antireflection coatings.

Figure 11 shows transmission data for a 260 Å thick ITO coating measured by the engineers at Meadowlark. There are two ITO coatings on each liquid crystal cell, for a total of 18 in the overall filters (figures 3 through 8). Note the coatings used on the liquid crystal cells in this filter are slightly thicker than the 260 Å coatings measured. These data were also included on figure 9. The losses due to improper index matching are not easily estimated, but are not more than a few percent at any given interface.

It is this combination of polarizer losses, ITO coatings, and other internal losses that determines the overall transmission of the filters. A review of the Meadowlark model reveals that the transmission of the polarizers and the ITO coatings were not included in their calculations. The poor transmission characteristics have been discussed with the engineers at Meadowlark and a number of suggestions have been made. These suggestions are discussed in the "Performance Improvement" section below.

Figure 12 shows the measured filter full width at half maximum (FWHM) transmission bandwidth as a function of center wavelength. In addition to the raw data, the plot also shows a linear regression of the data indicating the bandwidth is a linear function of wavelength. The regression parameters are: Slope = 0.0109 nm/nm and Y intercept = -3.001 nm. With these regression parameters, the FWHM bandwidth varies from about 1.56 nm at 420 nm to 3.1 nm at 560 nm. These values are consistent with the expected values of bandwidth predicted by the Meadowlark model. The model predicts the bandwidth would be given by a linear relationship

with the same slope, but a Y intercept of -2.807 nm resulted in predicted values of bandwidth of 1.83 nm at 420, and 3.37 nm at 560. The origin for this 0.27-nm offset is uncertain, but is probably because the equation used to estimate the bandwidth⁹ is derived from assuming the filter is made from a single type of birefringent material and does not take into account the dispersion (change in birefringence with wavelength) of the various materials used to construct this filter.

2. Out of Band

Spectral scans of the filter transmission as a function of wavelength were used to ensure the filter was tuning correctly and to calculate the relative energy passed in band to the amount of energy out of band. Early in the program, it was scans of this type that revealed that there was a problem in the filter driver software. A description of the scan procedures with a block diagram and equipment list are included as appendix B. Scans were taken from 400 nm to 600 nm even though the filter was only designed to scan between 420 nm and 560 nm. Figures 13, 14, and 15 are the results of these scans at 420 nm, 490 nm, and 560 nm, respectively.

From these scans, the following data were calculated:

λ Set (nm)	Bandwidth (nm)	Out-of-Band Energy (Arbitrary Units)	In-Band Energy (Arbitrary Units)	Ratio In Band/ Out of Band	Modeled Ratio
420	2.00	0.0840	0.0280	0.3350	0.2690
490	2.50	0.1730	0.2620	0.6620	0.1710
560	3.25	0.1910	0.5650	2.9410	0.1280

Note that the bandwidth values are only accurate to about 2 decimal places because of the spectral resolution of the monochromator being used. With the smallest available slits (0.25 mm), the Optronics Model 740 Monochromator has a spectral resolution of 0.5 nm.

Other things to note in these three figures are the peak transmission of the pass band and the free spectral range of the filter. For the filter set at 420 nm, the transmission is only 1.4%, while it approaches 11% at 490 nm and almost 18% at 560 nm. These transmissions are consistent with the losses due to the polarizers and the ITO coatings discussed above (figure 9). The position of the secondary maximums determine the free spectral range of the filter. The specifications given for the filter were that it tune from 490 nm plus or minus 70 nm and that it have a free spectral range of 140 nm. That is, the central peak should be capable of moving from 420 nm to 560 nm while the secondary peaks remain at least 140 nm on either side of the maximum.

In figure 14, the 420-nm scan, there are a pair of peaks between 400 nm and 420 nm that are technically outside the specified tuning range, but because of their relative strength and proximity to the central maximum, they would pose a problem for operating the filter at 420 nm. In addition, the first major secondary peak in the tuning range occurs at about 530 nm, only 110 nm from the main peak, and slightly less than the specified free spectral range of 140 nm. Both of these features are a result of the less than perfect calibration of the center frequency vs voltage tuning curves for most of the elements, and a calibration errors for element #2 (see below). When one or more of the elements is not perfectly adjusted to the desired wavelength, the secondary peaks begin to rise while the primary peak expands and begins to fall. This effect will be

discussed further in the section on temperature stability. In addition, the reduced free spectral range for the filter tuned to 420 nm may also be due to the dispersion of the birefringence of a number of the material used in the filter. This dispersion, or change in birefringence with wavelength, makes it very difficult to maintain the proper phase retardance across the entire tuning range.

The 490-nm and 560-nm scans are considerably better than the 420-nm scan. In both of the longer wavelength scans, there are no secondary maximum showing, although in the 560-nm scan there is a peak at 575 nm that is about 30% of the main peak. Note that the secondary maximum should have approximately the same transmission as the primary peak (after any differences in polarizer and ITO coating transmissions are accounted for), and should not be confused with the numerous small peaks that appear throughout the tuning range of the filter. These small out-of-band peaks are higher order transmission bands from the thicker elements that should be suppressed by the minima in the transmission spectra of the thinner elements. They are evident here due to a less than perfect match for the wavelength tuning of one or more of the elements. It is interesting to note that the lack of a secondary maximum in the 560-nm scan (between 560 nm and 400 nm) indicates a free spectral range of greater than 160 nm, considerably larger than the specified 140 nm.

3. Element Characterization

Each of the six elements of the filter were designed to operate independently, as well as being part of the entire filter. Figures 16, 17, 18, 19, 20, and 21 are spectral scans of the individual filter elements. Each element was scanned with the filter set to 490 nm. In addition to the measured data for the filter transmittance, there is a plot of the expected transmittance from the Meadowlark model. This modeled transmittance has been scaled by the measured polarizer and ITO transmissions (note that these are plots of transmittance (0–1) not transmission (0–100%)).

Two things to note in each of these plots are the relative position of the peaks around 490 nm in the measured data and the position of the minima on either side of the 490 nm peak. Since the filter was set at 490 nm, the measured data should peak at exactly 490 nm. However, for most of the scans, the peak in the measured data is shifted slightly from this position. This illustrates the temperature sensitivity of these devices. There was no active temperature control on the filter as the data was taken. Because of this, the peak transmission wavelength tended to drift as the ambient temperature drifted. The data for a single scan was taken in a matter of a few minutes, so the temperature stability over an individual scan is fairly good. However, scans were taken over the course of many days in the lab, so there may be considerable (up to 5°C) variation from scan to scan. The temperature of the filter during the scan is indicated in the legend of each plot. The filter was originally calibrated in the Meadowlark Optics, Inc., laboratory outside Boulder, Colorado, in mid-December, where the room temperature was a fairly constant 20°C. The farther the temperature varies from this calibration condition the more the transmittance peak shifts away from 490 nm. This temperature dependence and possible solutions are discussed in more detail below.

Another point of interest is the transmittance does not drop completely to zero at the nulls (points where $\phi = n\pi/2$) as it should. Since the crossed polarizer extinction ration for the Polaroid HN42HE is greater than 1000 for collimated light, one would expect the nulls to appear to be zero on the scale where they are being plotted. The fact that they are not indicates that some of

the polarized light is somehow losing its polarization as it passes through the filter, and this randomly polarized light is being partially transmitted through the exit polarizer as leakage. There are a couple of possible explanations for this effect. First, the beam out of the monochromator is not perfectly collimated. The output lens is designed to collimate the beam as much as possible over a limited depth of focus, but there will be some unavoidable divergence in the beam. This divergence may account for some of the leakage at the nulls¹⁰. The balance of the leakage may be due to scatter off of the liquid crystal devices and various surfaces in the element. Light that is scattered inside the element may still reach the exit polarizer, but it will have lost the polarization direction originally imposed on it by the entrance polarizer.

In the higher order filter elements (number 5, figure 20, and number 6, figure 21), this problem seems to be more severe, but actually this is an artifact of the resolution of the spectral data. All of the data in figures 16 through 21 were taken at 1-nm spacings, so in these higher order elements there are fewer data points per cycle (40 cycles in 200 nm, or 5 points per cycles for figure 21). Because of the small number of data points per cycle in these plots, the minimum transmission may actually occur between two data points, making it appear on the plot that the curve does not go all the way to zero. This "aliasing" effect is not a problem in the plot of the lower order elements where there are up to 400 points per cycle.

As a final point of interest, notice the relative spacing between the nulls for both the theory and the measured data. The spacing between the nulls is an indication of the retardance of the filter element (equation 1, $\phi_2 - \phi_1 = \pi$). If the measured spacing is slightly smaller than the predicted, as in figure 16, the actual retardance of the element is larger than expected. If, however, the spacing between the measured nulls is larger than the theory, the actual retardance is smaller than called for in the design.

Figure 17 is a similar plot for the second element. The data for this plot was generated after the second element was repaired at Meadowlark Optics, Inc. and recalibrated at NRaD (see section 4 below). Note that the peak in the measured data is close to 490 nm (since the voltage calibration was accomplished at about the same ambient temperature as the measurement), but the frequency of the curve is not correct; in particular, the theory curve has three distinct peaks across the 200 nm plotted, while the measured curve has three and a half peaks. This indicates a significant difference between the expected retardance and the actual retardance, and is due to the wrong choice of operating voltage on the LCVRs as discussed below. Recall that the cell was recalibrated at NRaD because the calibration done at Meadowlark Optics, Inc. was also for the wrong operating voltage, and when element #2 failed early in the program, a similar effect was measured. However, in the case of the element failure, it exhibited twice as many peaks as expected, indicating an element with only half of the expected retardance value. This anomaly was traced to a broken lead on one of the LCVRs, leaving the cell with only half of the designed retardance.

Unfortunately, after the error was noticed, there was no time to recalibrate the element at the proper operating voltage. This error in retardance will not affect the peak transmission of the filter, as the element is still calibrated to give a peak at whatever wavelength the filter is set at. It will result in substantial out-of-band leakage since the placement of the nulls for each element is calculated to block the second-order peaks from higher-order elements (see out-of-band measurements in previous section). The consequences of this error are discussed more fully in section 4 below.

Figure 18 show similar data for the third element. In this case, we again see the nulls that do not fall quite to zero, and a slight discrepancy between the measured and predicted retardance values, with the measured retardance being slightly smaller than expected.

Figure 19 is a plot of the measured transmittance of the fourth element. It shows the same characteristics that were evident in the first three plots: the nulls that do not quite fall to zero, and an oscillation frequency that is not quite the same as the predicted value. In addition, this is the first plot in which the predicted peak transmittance (scaled for polarizers and ITO coating losses) is greater than the measured peak transmittance. This trend continues in elements #5 and #6 as well. The reason that the theory underpredicts the peak transmittance in the first three elements, while overpredicting the transmittance in the last three, is not certain at this time. However, it may be related to the manner in which the retardance is achieved as explained in the physical description section above. Recall that in the last three elements, multiple peaks were used to span the tuning range, and the retardance of the liquid crystal elements was subtracted from the fixed retarders, while in the first three, a single peak was used to cover the entire tuning range, and the retardance of the liquid crystal devices was added to the fixed retarders.

4. Voltage vs Center Wavelength

By changing the peak-to-peak amplitude of the 2-kHz square wave that drives the LCVR, the retardance of the elements can be varied. Equations (1) and (2) show this causes the peak transmission wavelengths to shift. Though the LCVR are designed to have a specific retardance at a particular design voltage, the actual retardance and the movement of the transmission peaks must be calibrated empirically⁷. Most of these calibrations were performed at Meadowlark, and a file containing a look-up table of the voltages necessary to move a transmission peak to a particular wavelength was provided with the filter (appendix C). However, in July 1993, filter element #2 failed and had to be returned to Meadowlark where the LCVR was rebuilt. Because the liquid crystal cell had been rebuilt, Meadowlark also recalibrated it. When the new calibration data was reviewed by engineers at NRaD, it was discovered the element had been calibrated at a voltage that gave a retardance twice as high as the design retardance at 490 nm. Rather than return the element to Colorado for yet another calibration, engineers at NRaD chose to recalibrate the element for what they thought was the correct retardance at 490 nm. Unfortunately, they made an error and recalibrated for a retardance that was 1.5 times the design retardance (appendix D).

The consequences of this error are evident in figure 18, a plot of both the actual transmission of the element and the theoretical transmission. Although the peaks at 490 nm align fairly closely, the nulls in the theoretical curve fall at approximately 450 nm and 540 nm, while the nulls in the measured curve fall at 460 nm and 528 nm. As discussed above, while this calibration error will not affect the peak transmission at a programmed wavelength, it will result in significant degradation of the out-of-band rejection. This degradation is caused by the misalignment of the peaks and nulls of element #2 with respect to the other elements. The nulls from element #2 are no longer at the proper wavelength to suppress the peaks from element #3, and the secondary peaks of element #2 are not in position to be suppressed by the nulls of element #1. The effect is most obvious in figure 14, a scan of the filter transmission across the entire 400-nm to 600-nm range when the filter is set to pass 490 nm. The secondary peaks at 452 nm and 470 nm correspond to peaks from element #4 (figure 19). The 452-nm peak should have been blocked by a null from element #2 (figure 17), but was not because of the error in operating voltage for element #2. In addition, the 470-nm peak should have been blocked by a null in element #3 (figure

18); however, this peak is not completely blocked because the retardance of element #3 is slightly off as well.

This element could be recalibrated to eliminate the calibration error; unfortunately, the project has run out of time and money. The calibration process is included in the list of performance improvement suggestions.

5. *Field of View*

Field of view is a measure of the solid angle through which the filter will accept light rays. The angle is measured between the incoming ray and the surface normal to the entrance aperture or pupil (the optic axis in this case). The field-of-view angle defines the half angle of a cone. Any set of parallel rays that strike the front surface of the filter with a ray angle less than the field-of-view angle should be transmitted through the filter with at least 50% transmission. The physical dimensions of the filter restrict the maximum acceptable ray angles to less than 16.8 degrees (see figure 22, $\arctan [0.8''/2.655''] = 16.8^\circ$). However, it is common practice to define the field of view of an optical system as the angle at which the energy throughput has dropped by half. In the case of this geometry, that angle will be considerably less than the 16.8 degrees. The theoretical field of view can be calculated by methods similar to those used in calculating optical transfer functions¹¹. Using this method, you can calculate the overlap area as the entrance pupil is shifted with respect to the exit pupil. When this overlap area has reached one-half of the area of the entrance pupil, the system will transmit only half of the energy incident on the entrance pupil. This is, in effect, what happens as the incident angle of the light falling on the entrance pupil moves progressively farther and farther off axis. This model assumes that the filter has a uniform transmission over the entire aperture. For the geometry and dimensions of this filter, the overlap area drops in half if the exit pupil is shifted from the entrance pupil by 0.205 inch. This corresponds to a ray incident on the entrance pupil at an angle of 4.415 degrees (note that this method actually underestimates the field-of-view angle because it does not take into account the apparent elongation of the aperture as the filter is viewed from off axis). These two values (4.4 and 16.9 degrees) bracket the expected field-of-view angle.

In addition to the physical limitations imposed by the filter geometry, there are other effects that conspire to affect the field of view of the filter. Most of these effects are described in the references and include: the variation in retardance with incident angle for the LCVR¹¹; the variation in path length through the birefringent material⁵; the variation in transmission through the polarizer as a function of angle¹⁰; and finally, the effect already mentioned, possible nonuniform transmission over the face of the filter aperture (see next section). Many of these effects also cause a shift in center frequency as well as a reduction in peak transmission. For this reason, the spectral transmission of the filter was measured as a function of incident angle on both sides of the filter normal for angles out to 12 degrees.

During these measurements, the beam from the monochromator was expanded to overfill the entrance pupil of the filter. For simplicity, the filter was rotated with respect to the beam, rather than moving the entire monochromator setup to vary the incident angle. The filter was set for peak transmission at 490 nm throughout these measurements. The data taken are presented as both a three-dimensional surface plot of absolute transmission (figure 22), and as a series of contour plots of relative transmission (figures 23 through 26). It is necessary to use a series of contour plots because the data spans 200 nm in wavelength using 200 data points, but only plus or

minus 12 degrees in rotation (12 data points at any single wavelength). This results in a very poor aspect ratio if the data is presented on a single plot. Figures 23 through 25 span the entire 200-nm wavelength range with relatively high resolution, while figure 26 shows only the central maximum with a single contour at 50% transmission. Figure 26 allows a direct determination of the filter field of view which is plus or minus 7 degrees.

One effect to note on these contour plots is the growth of the out-of-band transmission peaks as the incident angle is varied. The origin of these peaks is discussed above, but the plots show that the wavelength at which they appear is dependent on the incident angle of the illumination. For rays incident on the filter from positive angles (see figure 22 for definition of positive and negative incident angles), the out-of-band peaks appear on the blue side of the central peak. This out-of-band leakage reaches about 20% of the peak transmission and is centered between 450 nm and 460 nm. While for negative incident angles, the out-of-band peaks reach 25% of the peak transmission, but appear on the red side of the main peak at wavelength between 545 to 550 nm.

Since the leakage pattern for crossed polarizers has two-fold axial symmetry¹⁰ and the variation in path length in the birefringent materials always makes the path length longer, increasing the retardance and shifting the peak wavelengths towards the blue, we can deduce from the asymmetric out-of-band leakage that the leakage must be due to the variation in retardance as a function of incident angle⁷. This is the only effect that can account for leakage in the blue when the light comes from one angle, and leakage in the red when the light is incident from the identical angle on the other side of normal.

6. *Transmission Uniformity*

The transmission uniformity measurements were designed to quantify the variations in relative transmission across the filter aperture. These measurements were performed with a frequency-doubled, diode-pumped neodymium:yttrium aluminum garnet (Nd:YAG) laser. The laser was used to provide a well-collimated, high-intensity light source with a small spot size. The filter was tuned to 532 nm to provide maximum transmission at the laser frequency. As in the field-of-view experiments, it proved easier to move the filter than move the laser beam.

The beam was aligned to strike the front surface of the filter at normal incidence. This ensured a consistent path length through the filter. The filter was mounted on two orthogonal Newport translation stages allowing translation in both axis perpendicular to the direction of the laser beam. With this arrangement, the filter could be moved in both the X and Y directions. Measurements of the filter transmission were then made over the face of the filter. These measurements were made over a regular grid with spacing of 0.05 inch. The transmission of the filter was measured at each step by measuring the energy in the transmitted beam and comparing it to the incident beam. To avoid errors caused by a fluctuation in laser power during the course of the measurement, part of the beam was diverted into a second photodetector, and the ratio of the energy in the transmitted beam to the energy in the diverted beam was recorded. After these data were collected, they were normalized to the largest value recorded, and plotted as relative transmission. These data are presented as a contour plot in figure 28.

The plot shows considerable variation in transmission over the face of the filter. Though a majority of the filter exhibits transmission of 70% or higher, the lower right quadrant ($0 < X < 0.4$, and $0 < Y < 0.4$) shows transmission in the 60% or lower range. This area of the plot

corresponds to measurements taken through the area where element #2 is experiencing significant delamination (see discussion above).

6. *Tuning Speed*

Several unsuccessful attempts were made to measure the time required for the filter to switch from one pass band wavelength to another. The measurements used two lasers passing through the filter simultaneously, the doubled Nd:YAG laser mentioned above, and an argon ion laser operating at 488 nm. The signals from both lasers were monitored on a photodiode while the pass band wavelength filter was switched from one wavelength to the other. Unfortunately, the response time of the diodes proved considerably slower than the switching time of the filter. When the measurements were attempted with fast photodiodes, the alignment proved to be too difficult for successful measurements. These measurements were abandoned as the project ran out of time and money at the end of FY 93.

An estimate of the switching speed can be made with a knowledge of the filter drive voltage. This drive voltage is a 2000-Hz square wave. To change the pass band frequency, the amplitude of this drive signal must be changed. However, the drive electronics are not capable of changing the amplitude in midcycle, so the minimum switching time would be one-half of a cycle for this 2-kHz square wave, or 0.25 milliseconds. This is considerably faster than the nominal switching times for LCVR that are usually on the order of a few tens of milliseconds⁷.

TEMPERATURE STABILITY

During the course of transmission measurements, considerable variation in peak transmission was noted between various data sets. This variation was traced to the change in operating temperature of the filter as the ambient temperature of the air changed. Figure 29 shows data taken at four different times, and the filter temperature is recorded in the legend. The data shows the peak transmission falling from a high of 11% at the lowest temperature (22.7°C) to a low of 9% at a temperature only 2.3°C higher.

The variation in transmission can be traced to variations in the retardance of the various elements as the temperature of the elements change. The birefringence of both the liquid crystal and the quartz are temperature dependent. This temperature dependence will affect each element in a slightly different manner, as they each have different amounts of liquid crystal or quartz in them. As there was almost a 20% decrease in transmission for only a 2.3°C change in temperature, it would be desirable to control the temperature of the filter to a fraction of a degree centigrade.

CONCLUSIONS

The results of this project were both encouraging and disappointing. On one hand, we were able to produce a tunable filter with a nominally 2-nm bandpass that tuned anywhere in the blue-green. Unfortunately, the overall transmission, out-of-band rejection, and temperature stability of the filter were rather poor. It is important, however, to differentiate between problems that are fundamental and conceivably insoluble and those that are just the result of poor engineering.

In the latter category, we can place the problems of temperature stability and out-of-band rejection. Most out-of-band problems would be resolved if element #2 were recalibrated to operate at the proper voltage. However, each of the elements showed a slight difference between their modeled performance and measure performance. As explained in the theory section, the out-of-band performance of the Lyot design is extremely sensitive to the placement of these peaks and valleys. Most of these differences were due to small variations between the expected and actual retardance of the elements. With a little careful "fine-tuning" of the design, most of these problems can be overcome.

The temperature stability problem has already been addressed by Meadowlark (explained below in the improvements section). By incorporating a thermostatically controlled heater, the filter can be held at a stable temperature above the ambient. This should allow consistent performance through a range of external temperatures, as long as the filter is properly calibrated to operate at this temperature.

The poor peak transmission is another issue altogether. Because of the nature of the Lyot design, a large number of polarizers are necessary. Considerable time and effort has been expended by other agencies, and on other programs, to improve polarizer efficiency. The Polaroid HN42HE polarizer was specifically designed by Polaroid for this type of application¹³ and is arguably the best available for the application, but they are simply inadequate.

One solution may be to bleach the polarizers⁸, but even this extreme measure does not hold the promise of as much as a factor of 2 improvement in transmission. An alternate solution may be the use of the Solc design that requires more birefringent elements, but considerably fewer polarizers. This design has been rejected in the past because the increase in the number of birefringent elements usually implies a large increase in costs. However, with the use of the relatively inexpensive polymers, or liquid crystal cells as birefringent elements, the increased cost may be manageable.

PERFORMANCE IMPROVEMENT/ FUTURE WORK

1. The peak transmission of the filter can be improved in a number of ways:
 - a. Meadowlark is already developing an improved ITO coating that is not as lossy at the blue end of the spectrum.
 - b. There are ITO coatings on the liquid crystal cell that are being used as a fixed birefringence device in element #3. These coatings are unnecessary and could be removed.

c. Considerable research has been done on bleaching Polarizer material to improve its transmission without significantly degrading its polarization efficiency⁸. Some of these methods could be applied to the polarizers used here.

d. The \dot{S} oic design has only two polarizers and has inherently better transmission.

2. The out-of-band transmission can be greatly improved by recalibrating element #2 for the correct operating voltage and by ensuring the retardance of each element is as close as possible to the theoretically required value.

3. As explained earlier, four of the six elements are experiencing some amount of delamination. The transmission uniformity measurements show that the transmission of the filter is significantly degraded in areas where the filter has begun to delaminate. Meadowlark is aware of this problem and claims that the delamination is due to failure of the cement that was used to bond the elements. Since this filter was produced, they have begun using a new brand of cement that they believe will significantly improve the durability of the filter. This new cement was use on element #6 when it was repaired in August, and it has held up well so far. In light of this, the other five elements of the filter should be rebuilt using the new cement in an attempt to improve the transmission uniformity.

4. The filter definitely needs active temperature control. As explained above, since this unit was built, Meadowlark has modified the design to include a heating element and temperature controller. By heating the filter above ambient, and incorporating an active thermostatic heater controller, the temperature can be maintained and stabilized to within a degree Celsius.

REFERENCES

1. Title, A. M., and W.J. Rosenberg. "Spectral Management," Journal Unknown.
2. Lyot, B. *Comp. Rend. Acad. Sci.*, vol 197, p. 1593, 1933.
3. Šolc, I. *Casopis Fysiku* [printed in Czech], vol 3, p. 366, 1953.
4. Title, A. M., and S. A. Schoolman. "Recent Advances in Birefringent Filters," *SPIE*, vol 88, Polarized Light, 1976.
5. Title, A. M., and W.J. Rosenberg. "Improvements in Birefringent Filter. 5: Field of View Effects," *Applied Optics*, vol 18, no. 20, 15 October 1979.
6. Title, A. M., and W.J. Rosenberg. "Tunable Birefringent Networks," *SPIE*, vol. 202, Active Optical Devices, 1979.
7. Gilman, S. et.al. "Properties of Tunable Nematic Liquid Crystal Retarders," *SPIE*, vol. 1166, Polarization Considerations for Optical Systems II, p. 461, 1989.
8. Gunning, W. J., and J. Foschaar. "Improvements in the Transmission of Iodine-Polyvinyl Alcohol Polarizers," *Applied Optics*, vol. 22, no. 20, p. 3229, 15 October 1983.
9. Yariv, A., and P. Yeh. "Optical Waves in Crystals," p. 151, J. Wiley & Sons, 1984.
10. Baxter, L., II. "On the Properties of Polarization Elements as used in Optical Instruments III. Angular Aperture Functions of a Positive Dichroic Film Polarizer," *Journal of the Optical Society of America*, vol 46, no. 6, p. 435, June 1956.
11. See for example, Goodman, Joseph W. "Introduction to Fourier Optics," p. 119-120, McGraw-Hill, 1968.
12. Yeh, P. "Dispersive Birefringent Filters," *Optics Communications*, vol. 37, no. 3, May 1981.
13. Racich, J., N. Schuler, and G. Trapani. "High Efficiency Polarizers for the Visible Region," *SPIE*, vol 464, Solid State Optical Control Devices, p. 104, 1984.

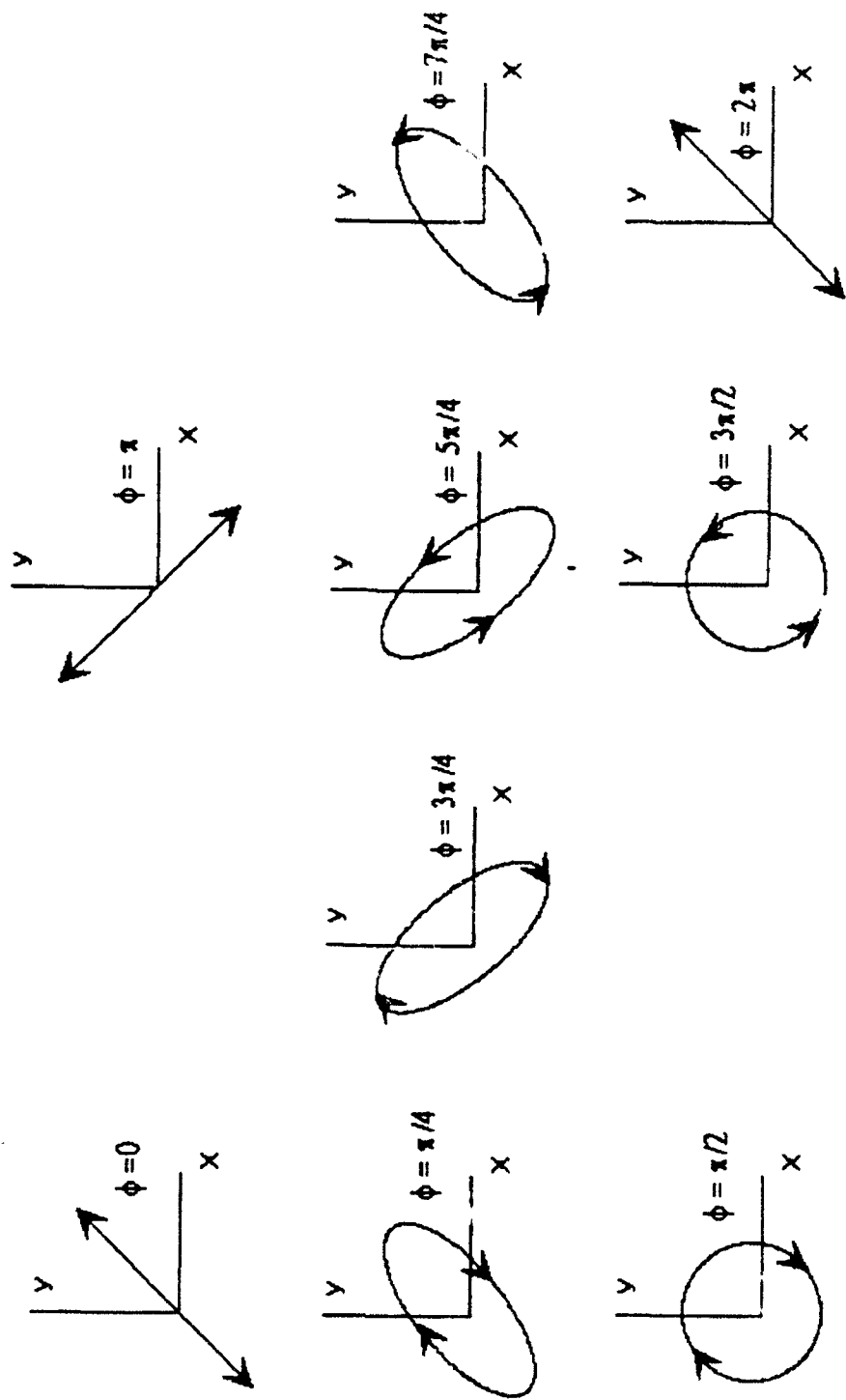


Figure 1. Polarization forms as a function of phase angle (ϕ).

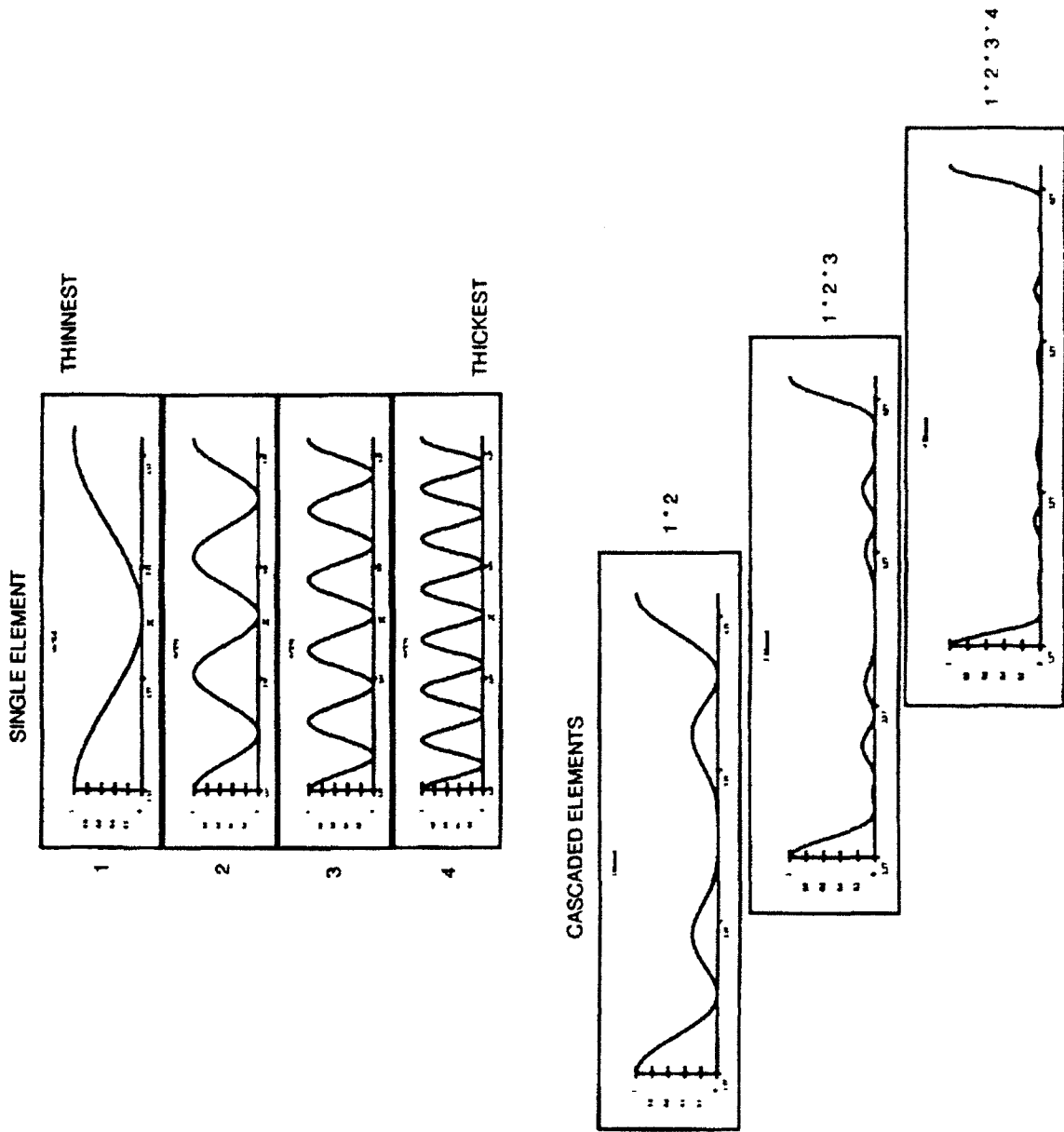


Figure 2. Transmission for Lyot filter.

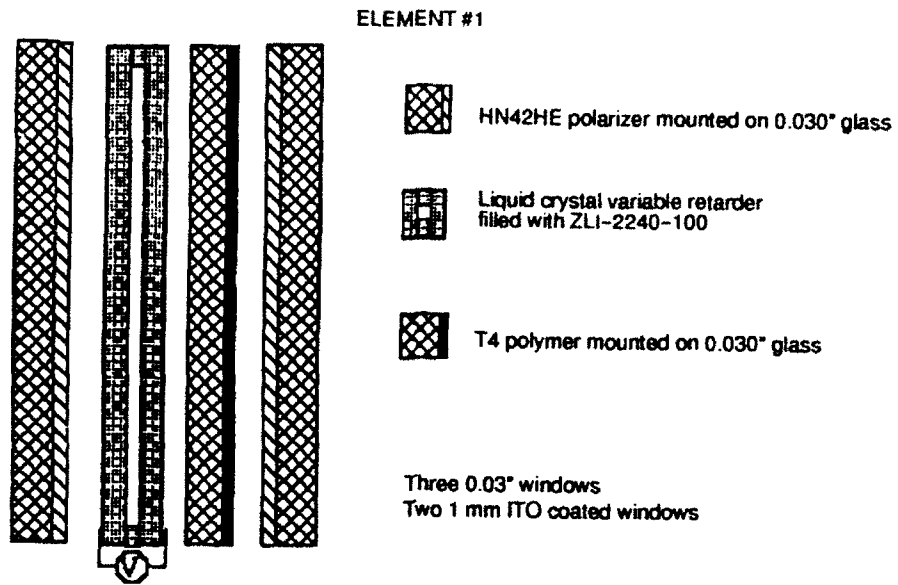


Figure 3. Filter element #1.

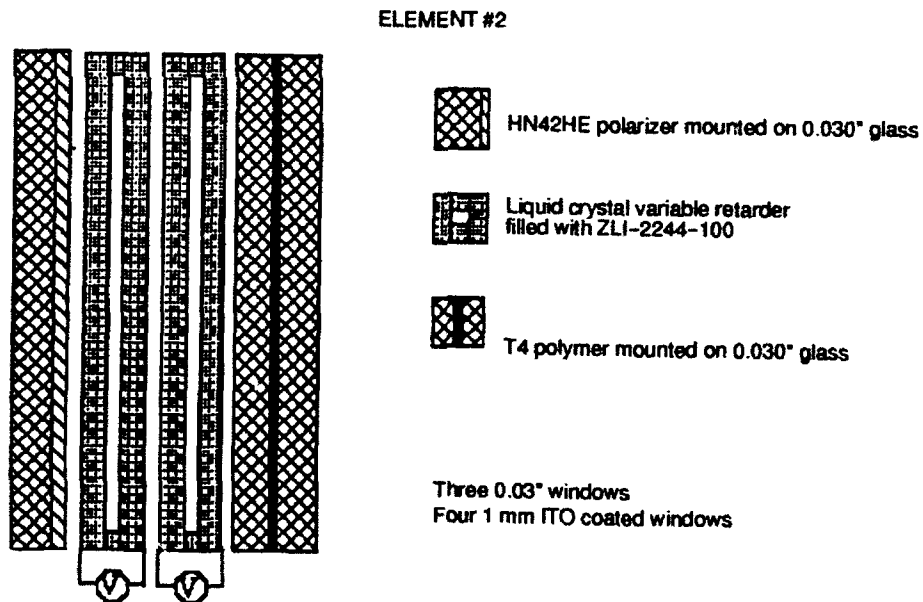


Figure 4. Filter element #2.

ELEMENT #3

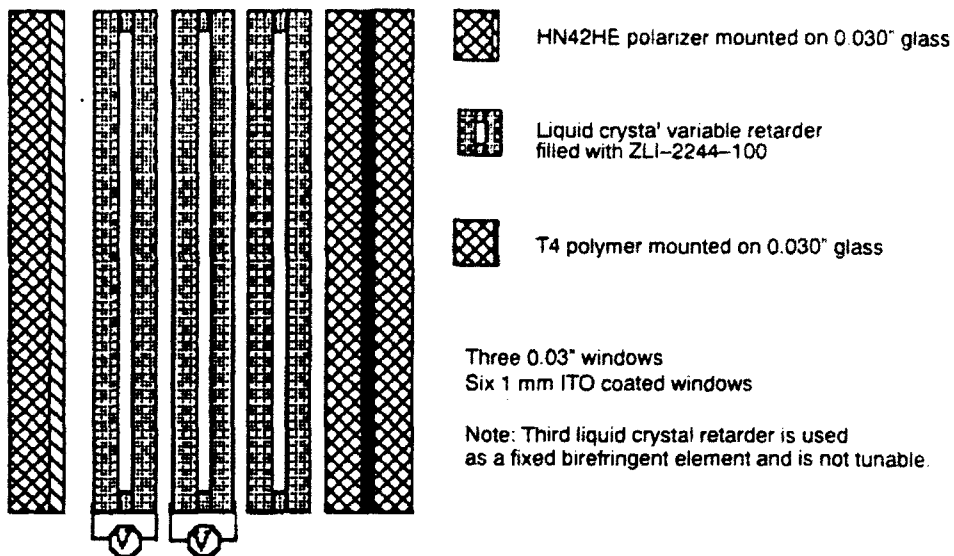


Figure 5. Filter element #3.

ELEMENT #4

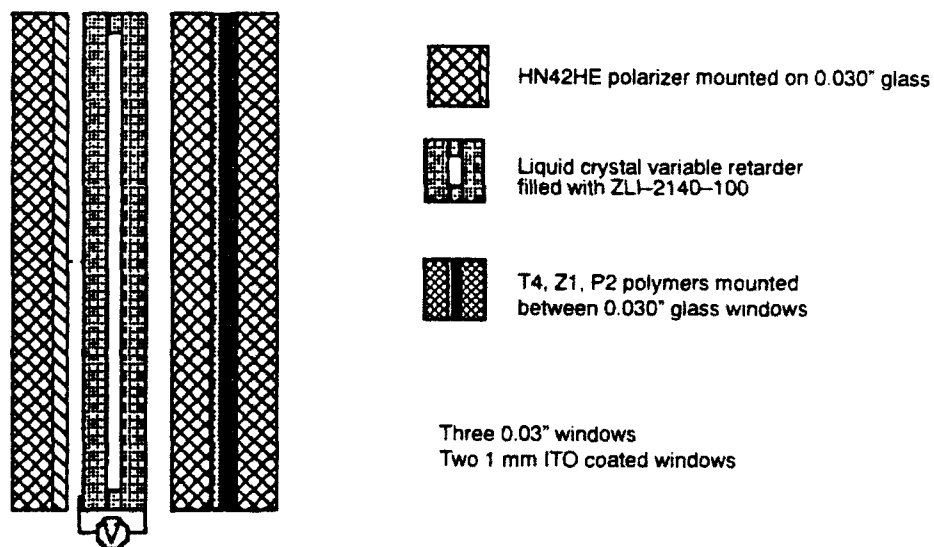
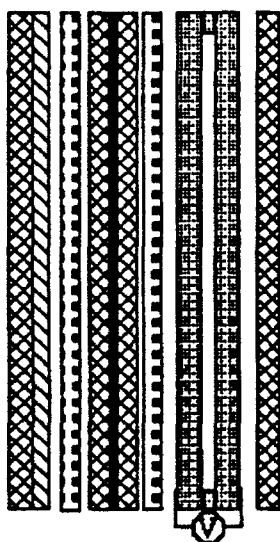


Figure 6. Filter element #4.

ELEMENT #5

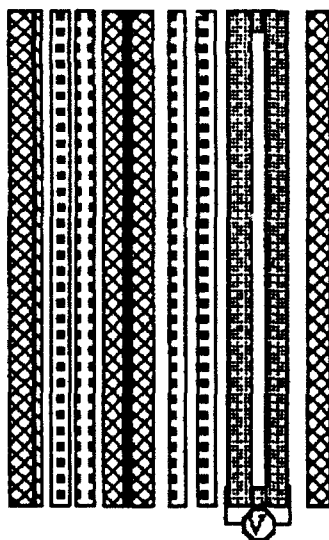


-  HN42HE polarizer mounted on 0.030" glass
-  1.12 mm quartz multiorder retarder
-  Z1 polymers. A chromatic half-wave plate between 0.030" glass windows
-  Liquid crystal variable retarder filled with ZLI-2140-100
-  0.03" window

Four 0.03" windows
Two 1 mm ITO coated windows

Figure 7. Filter element #5.

ELEMENT #6



-  HN42HE polarizer mounted on 0.030" glass
-  1.12 mm quartz multiorder retarder
-  Z1 polymers. A chromatic half-wave plate between 0.030" glass windows
-  Liquid crystal variable retarder filled with ZLI-2140-100
-  0.03" window

Four 0.03" windows
Two 1 mm ITO coated windows

Figure 8. Filter element #6.

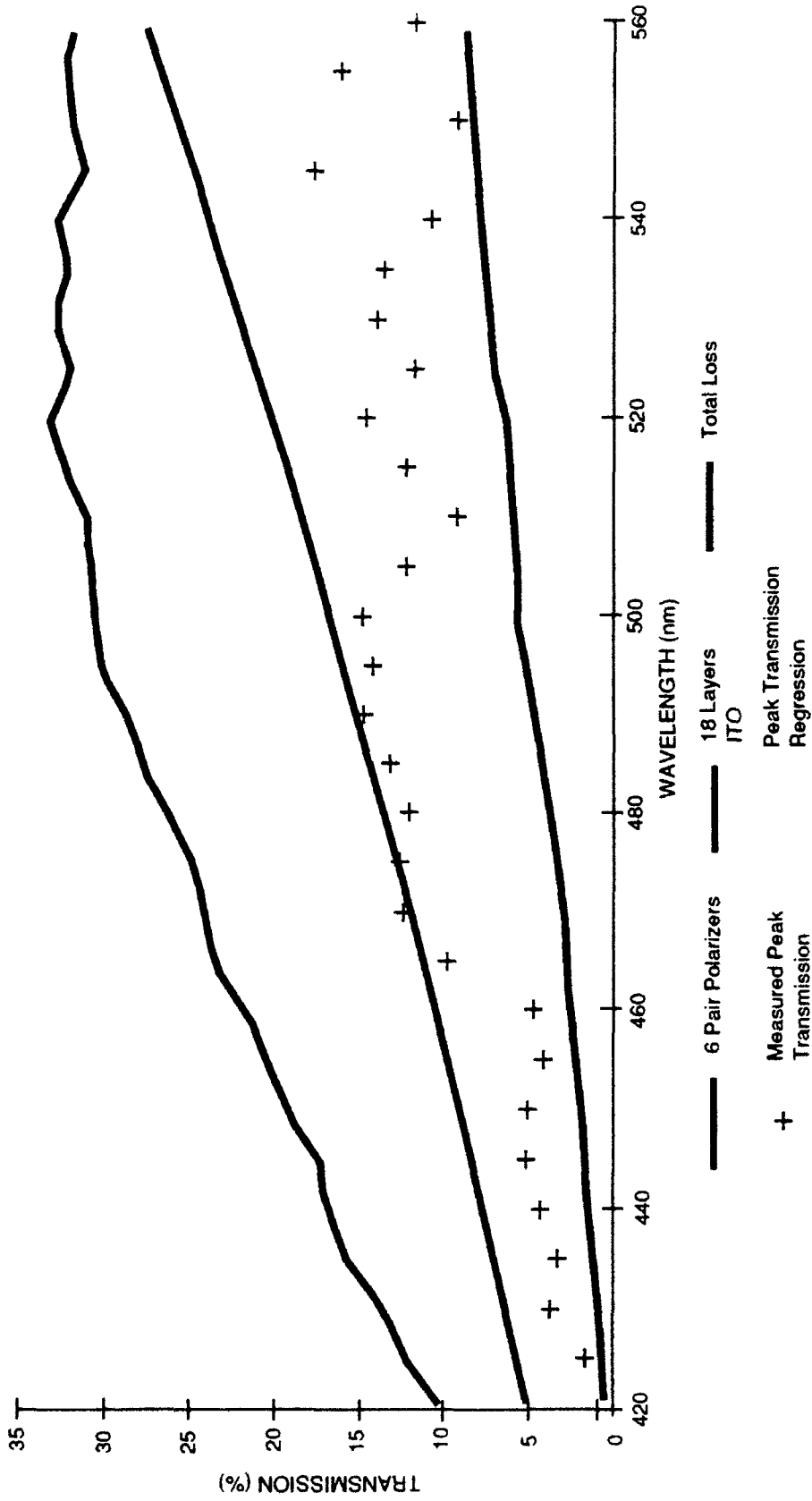


Figure 9. Peak transmission vs wavelength, and various contributions to the filter transmission.

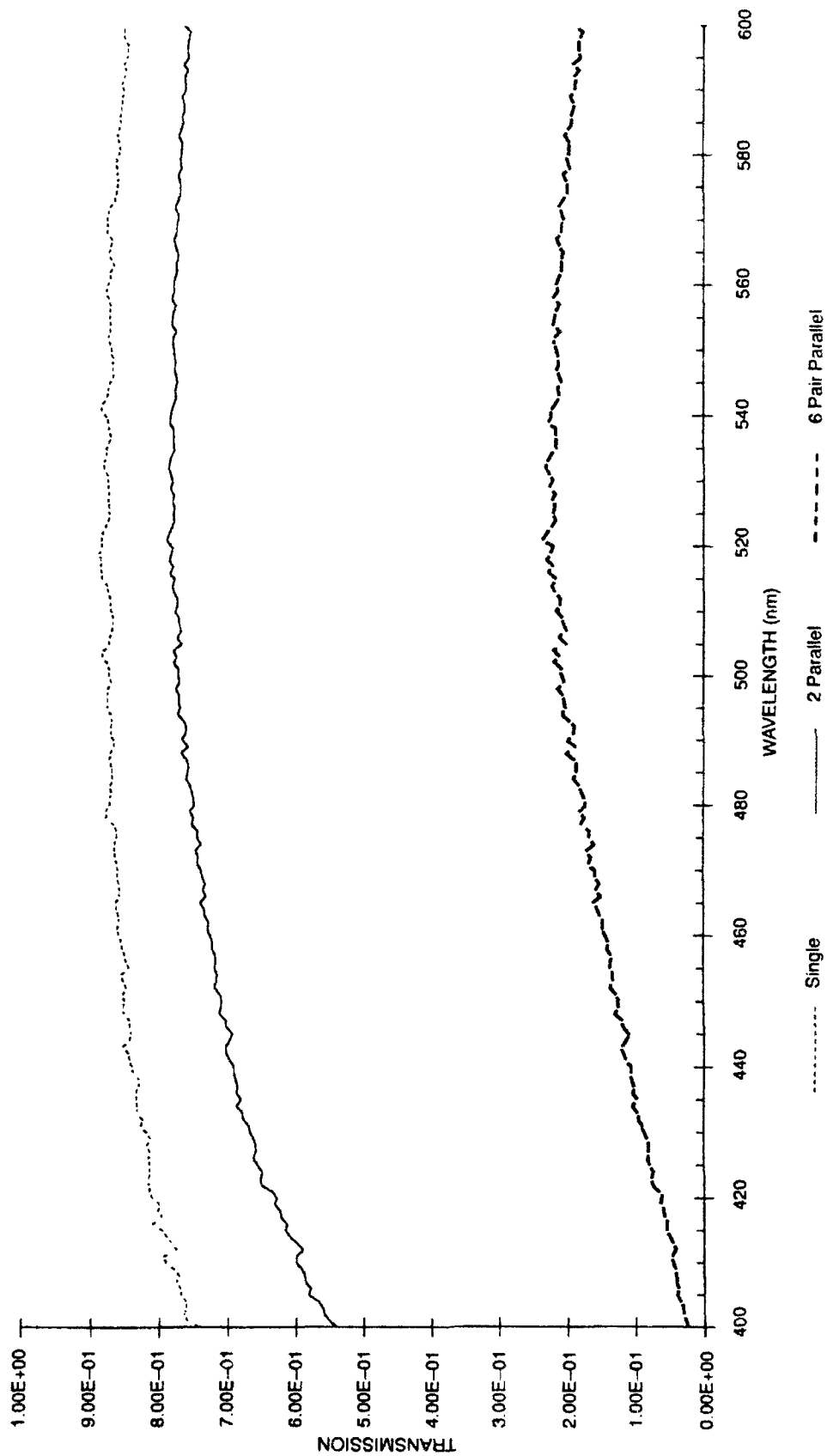


Figure 10. Polarizer performance.

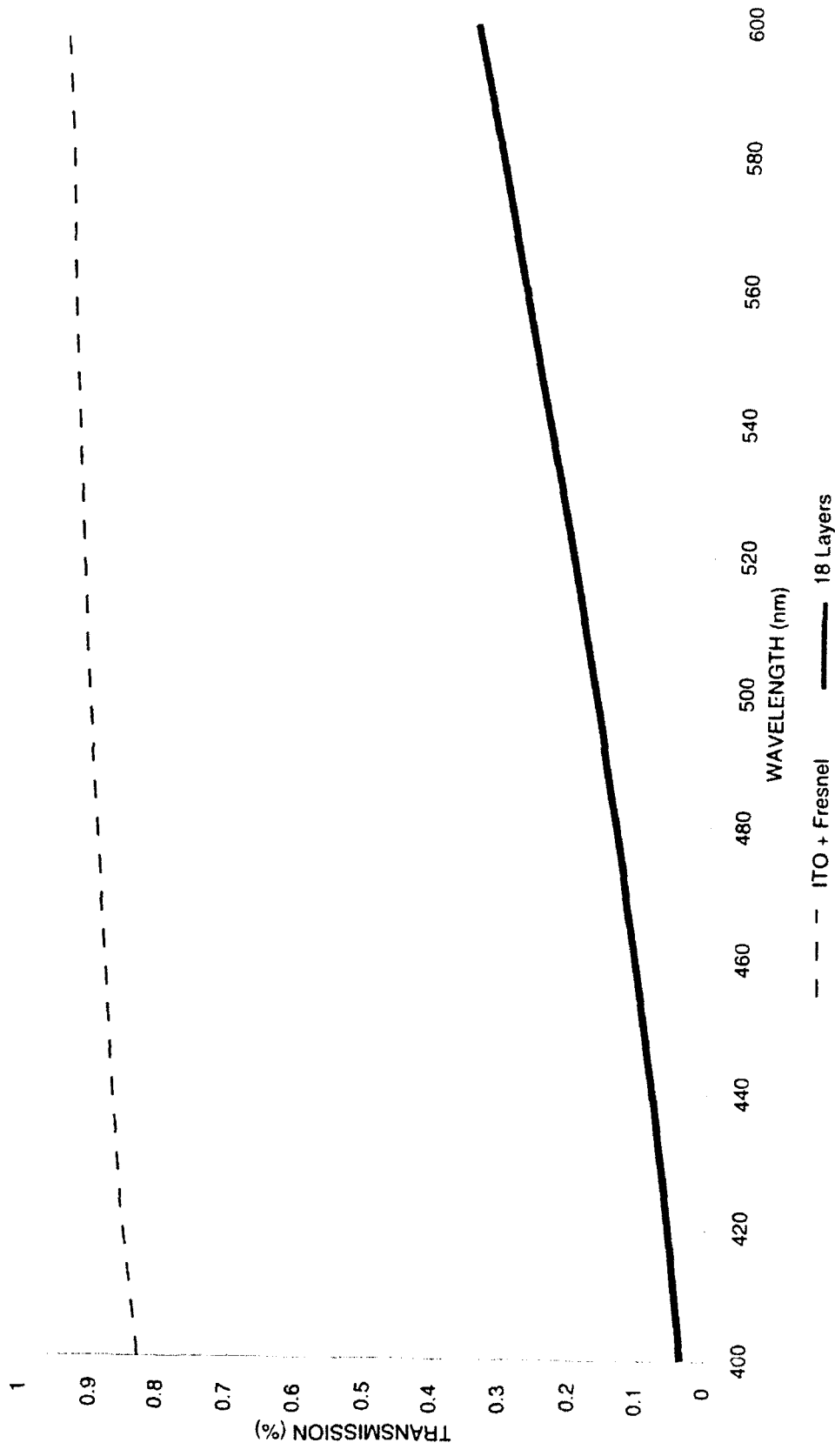


Figure 11. Indium tin oxide (ITO) coating transmission.

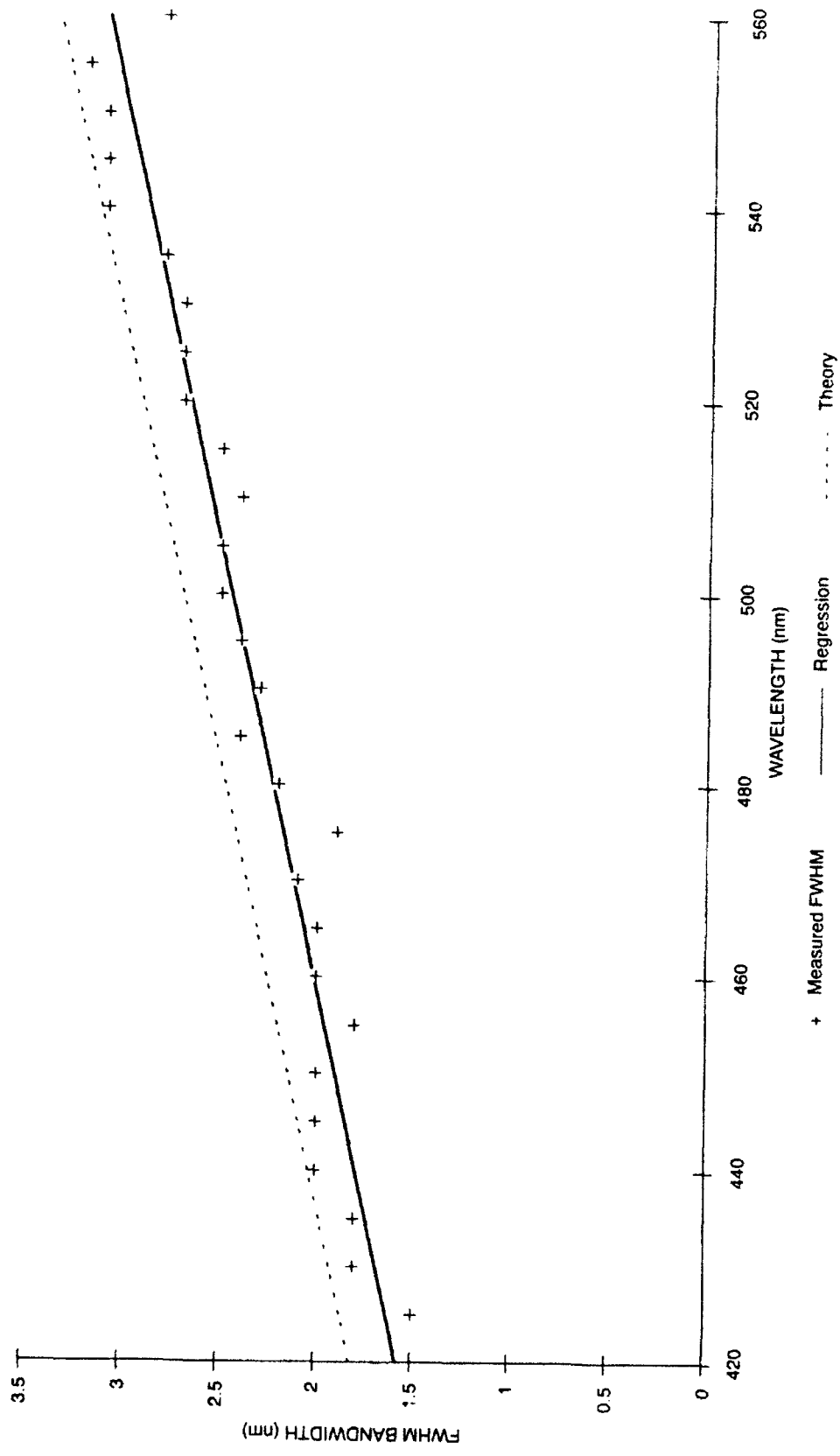


Figure 12. Filter band pass, measured and modeled data.

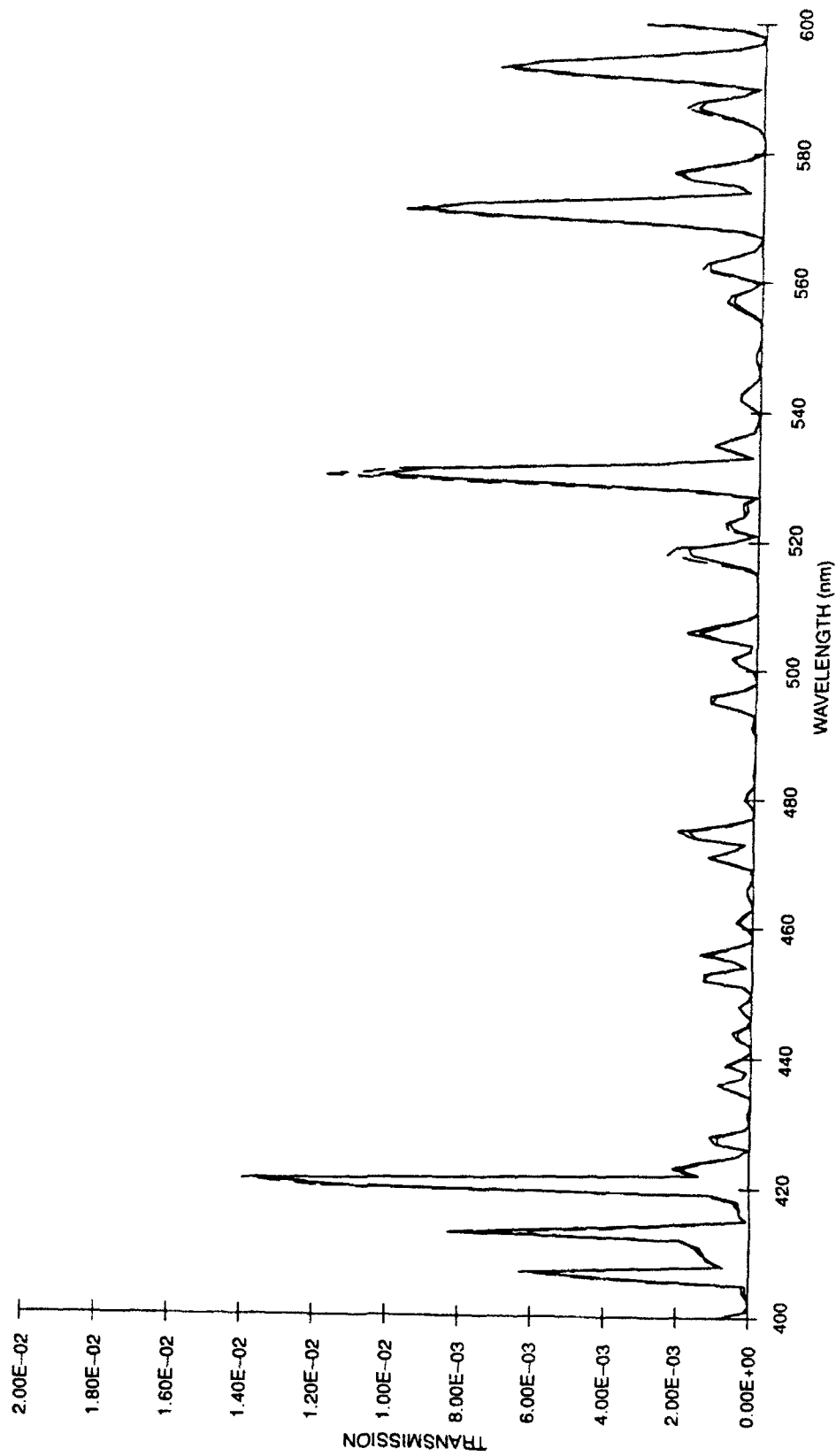


Figure 13. Filter transmission spectrum, filter set at 420 nm.

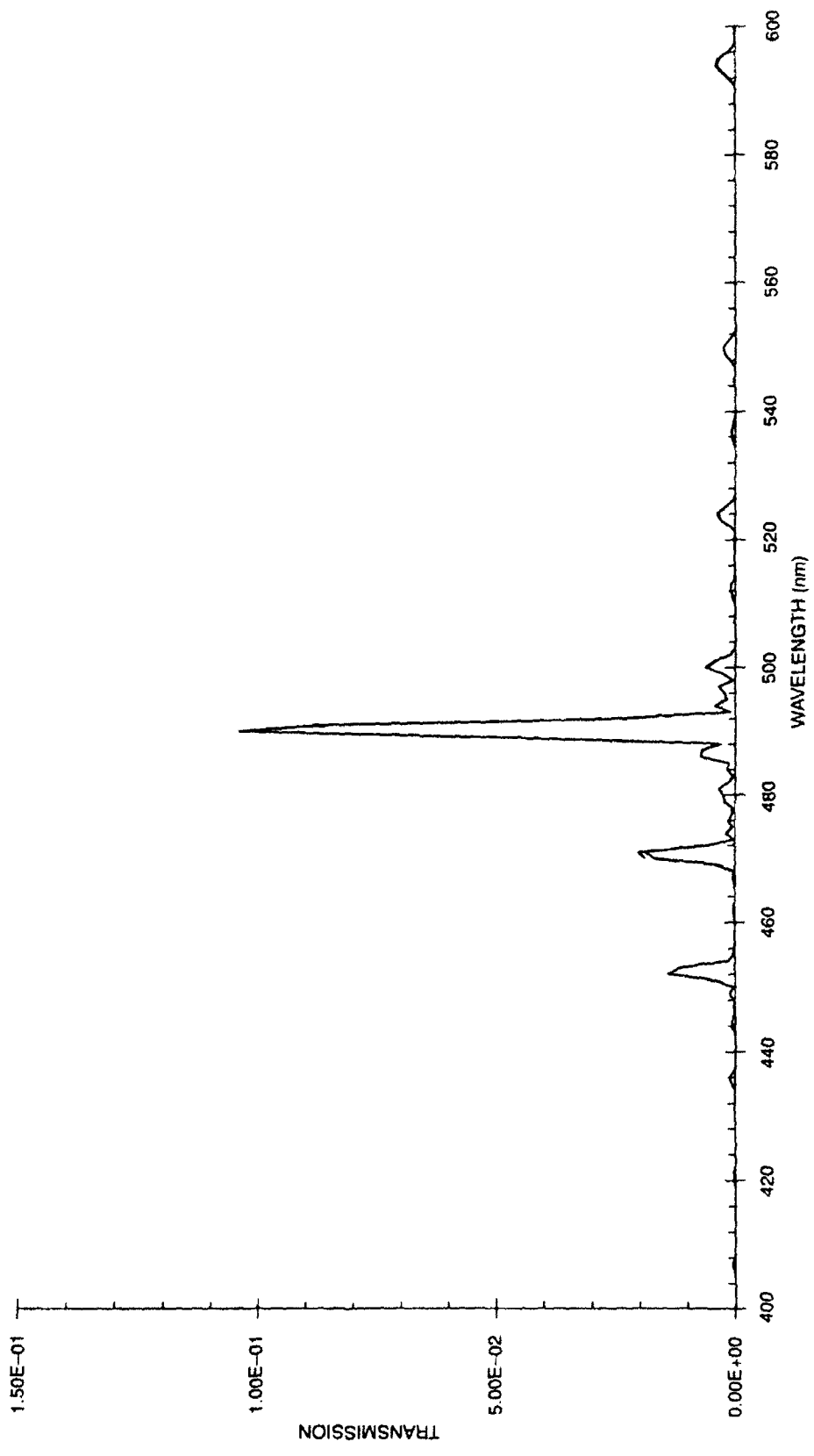


Figure 14. Filter transmission spectrum, filter set at 490 nm.

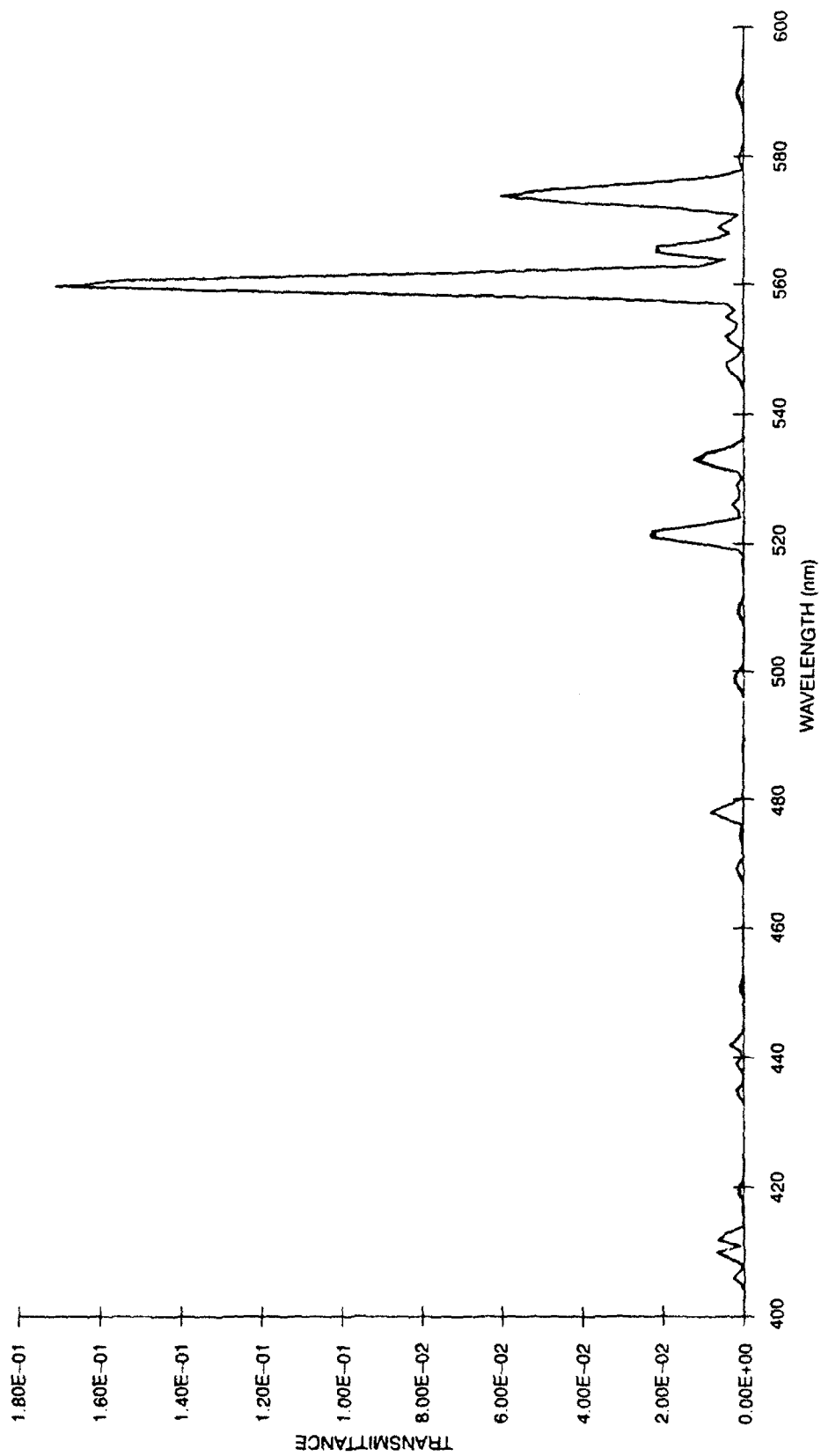


Figure 15. Filter transmission spectrum, filter set at 560 nm.

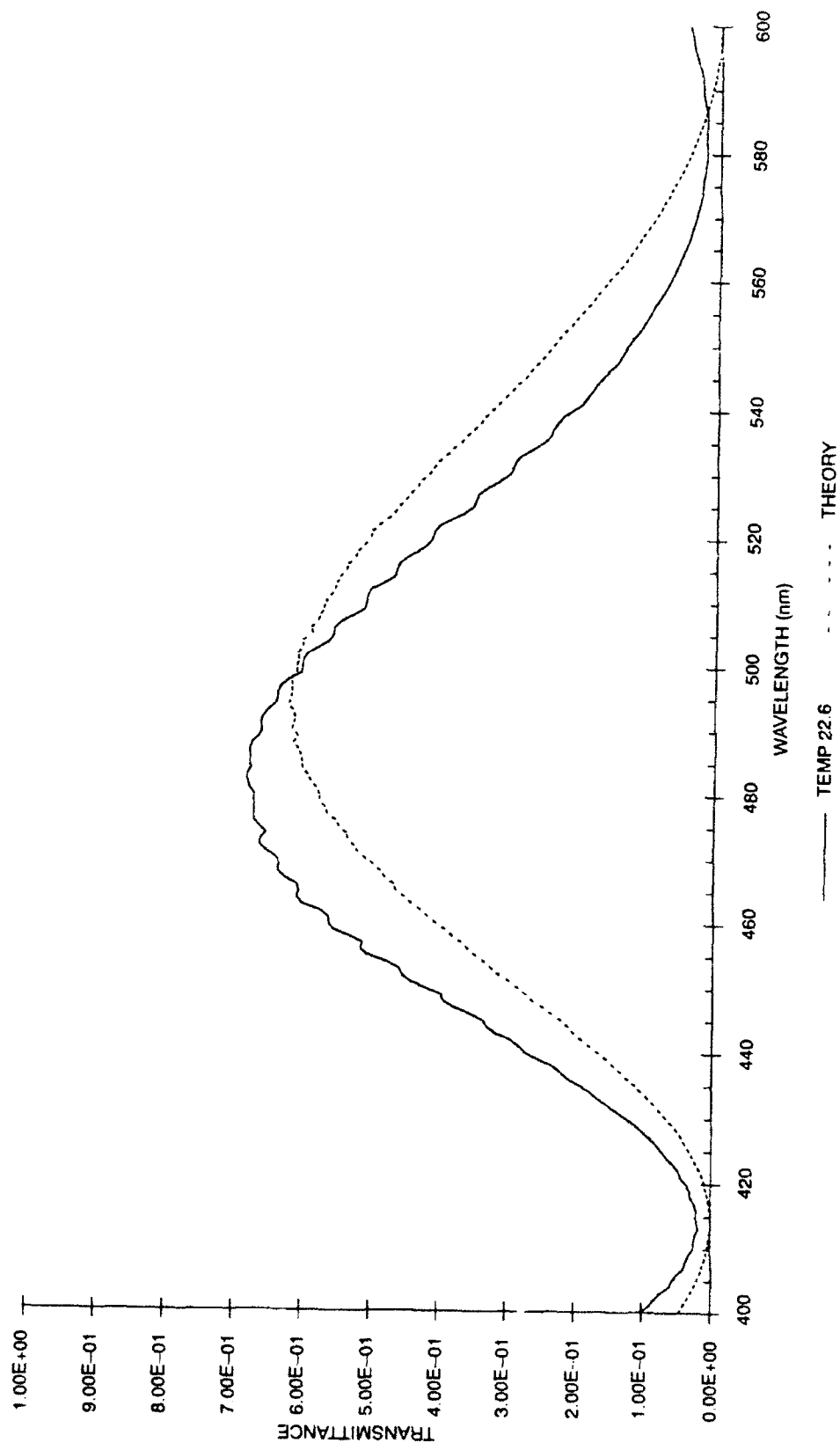


Figure 16. Single element transmission, measured and modeled, element #1.

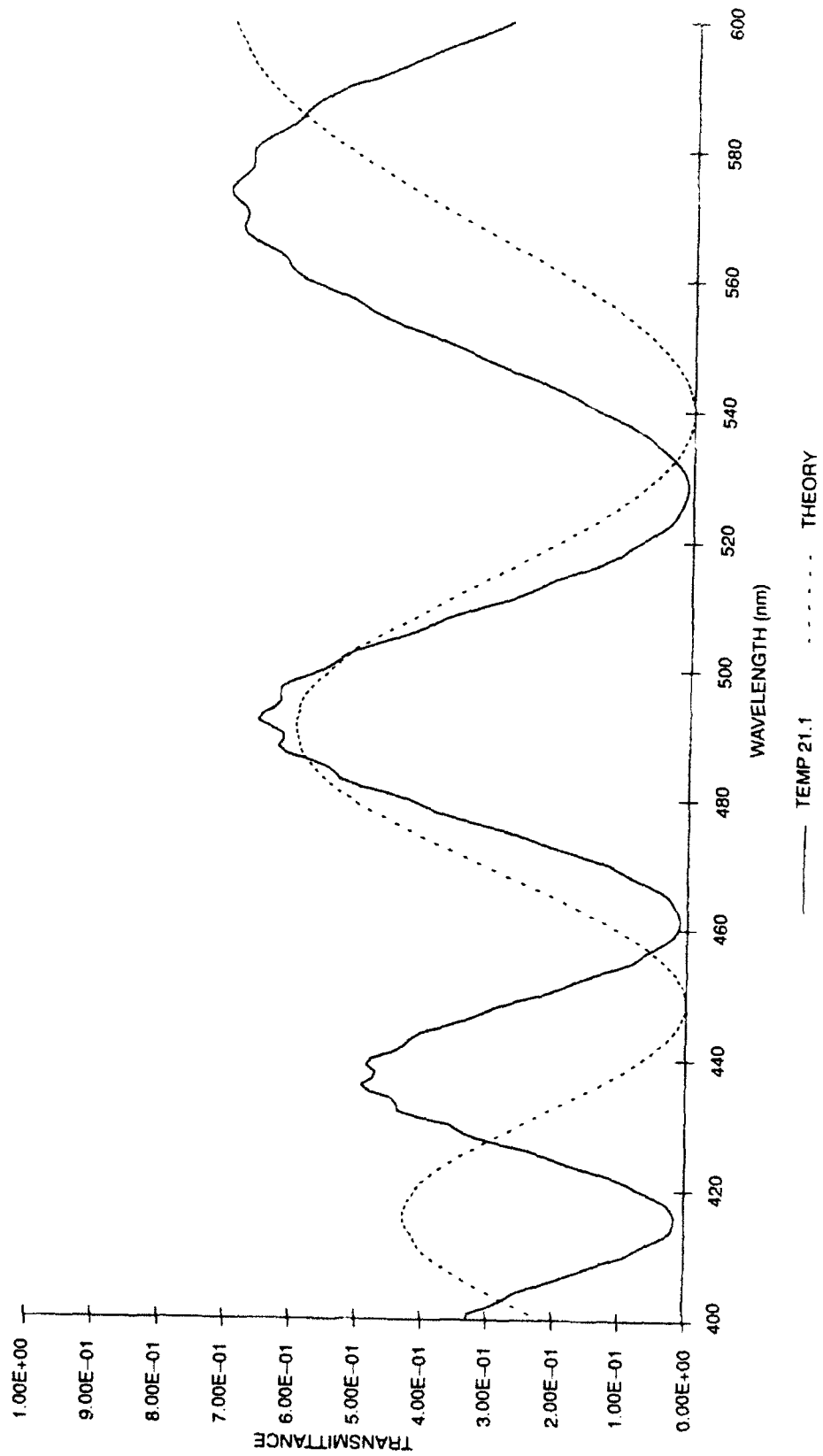


Figure 17. Single element transmission, measured and modeled, element #2.

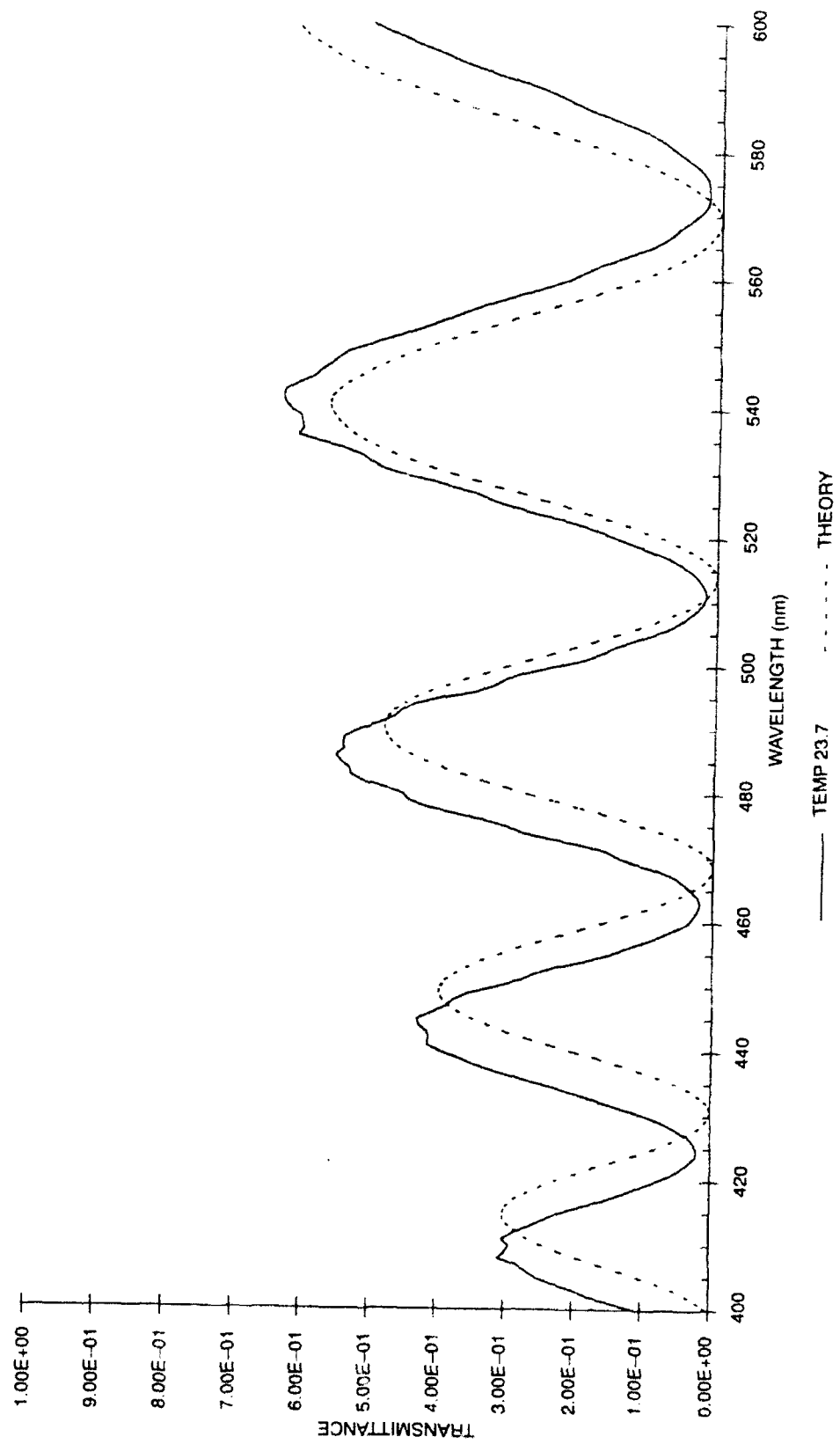


Figure 18. Single element transmission, measured and modeled, element #3.

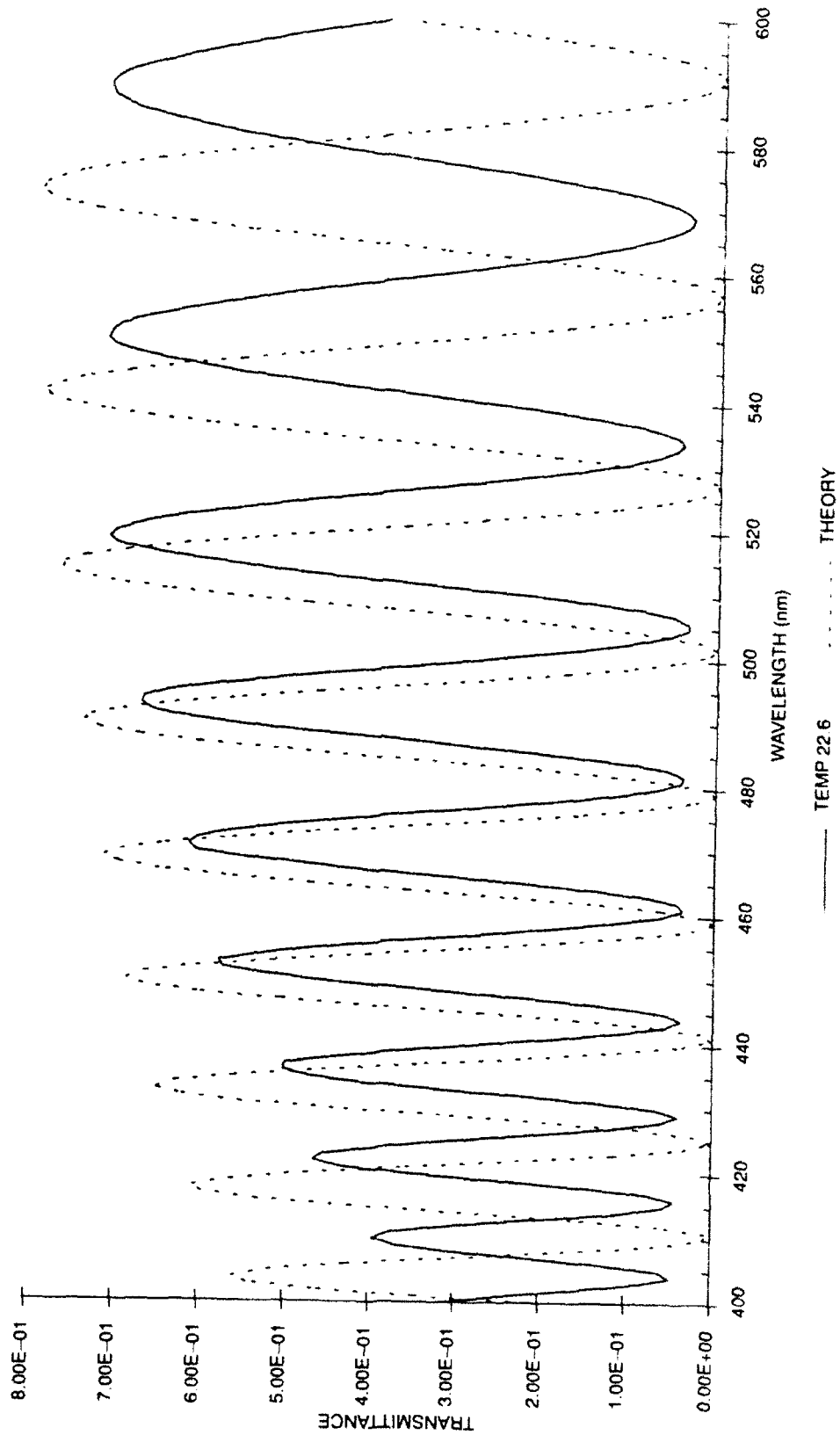


Figure 19. Single element transmission, measured and modeled, element #4.

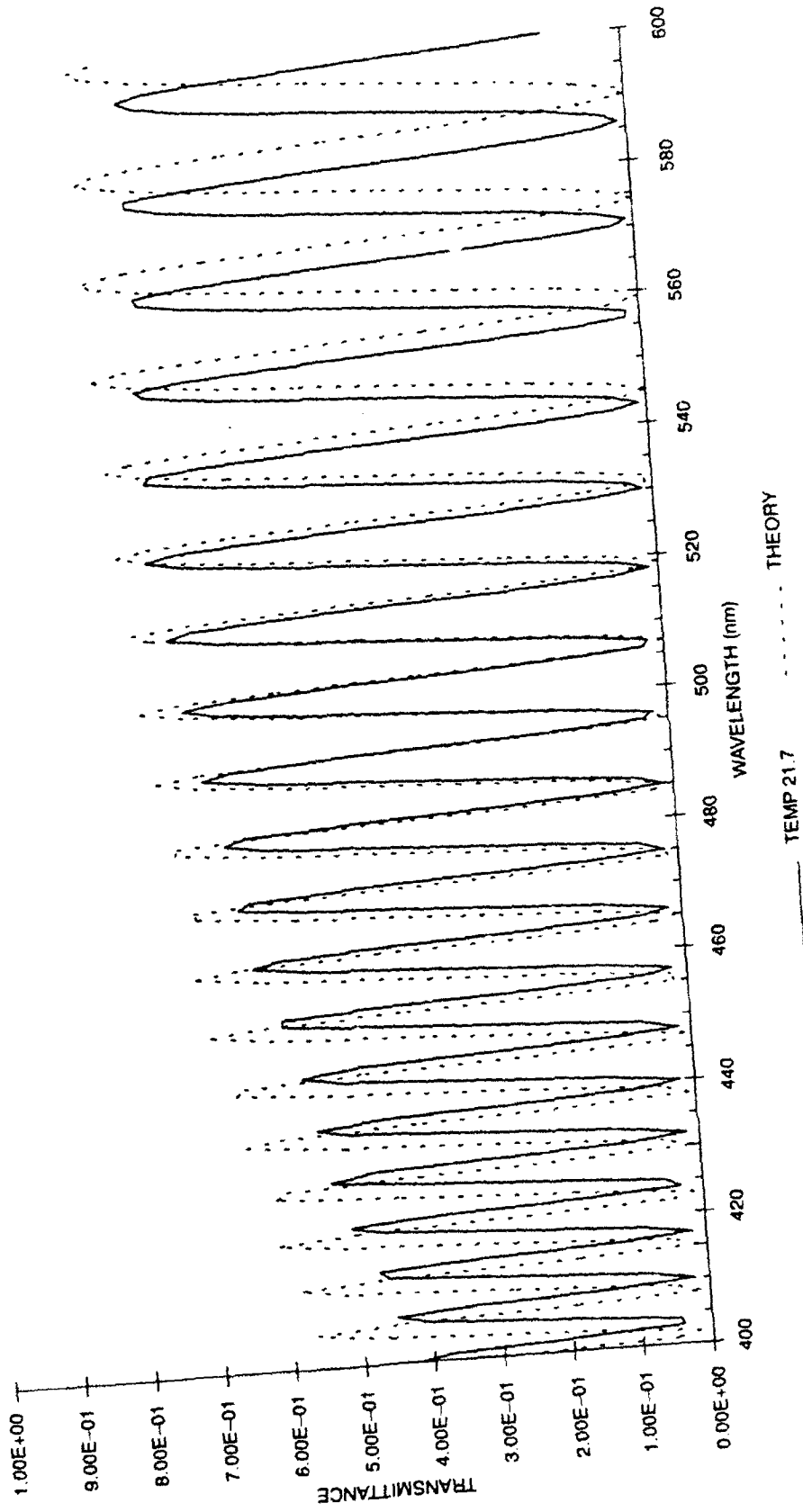


Figure 20. Single element transmission, measured and modeled, element #5.

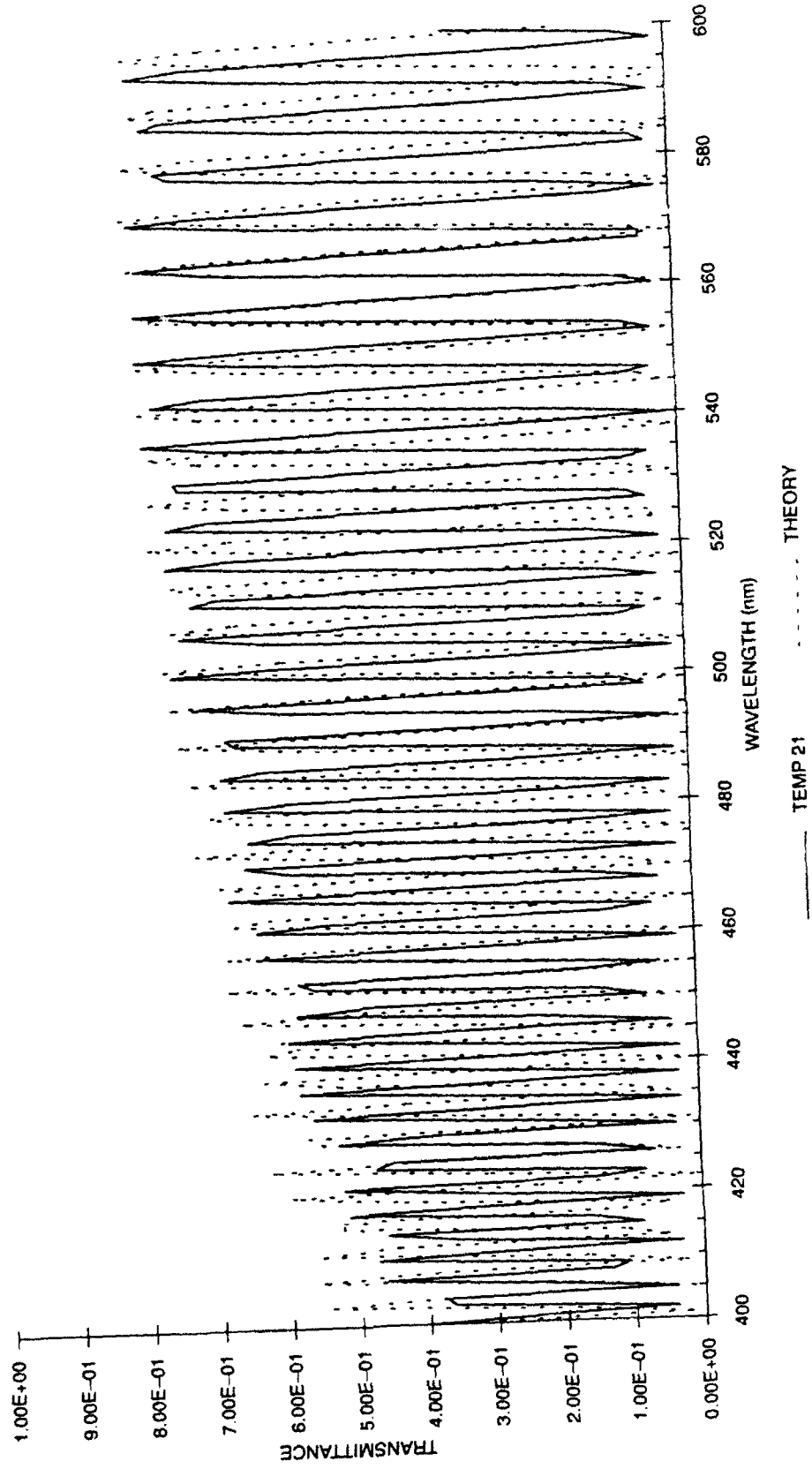


Figure 21. Single element transmission, measured and modeled, element #6.

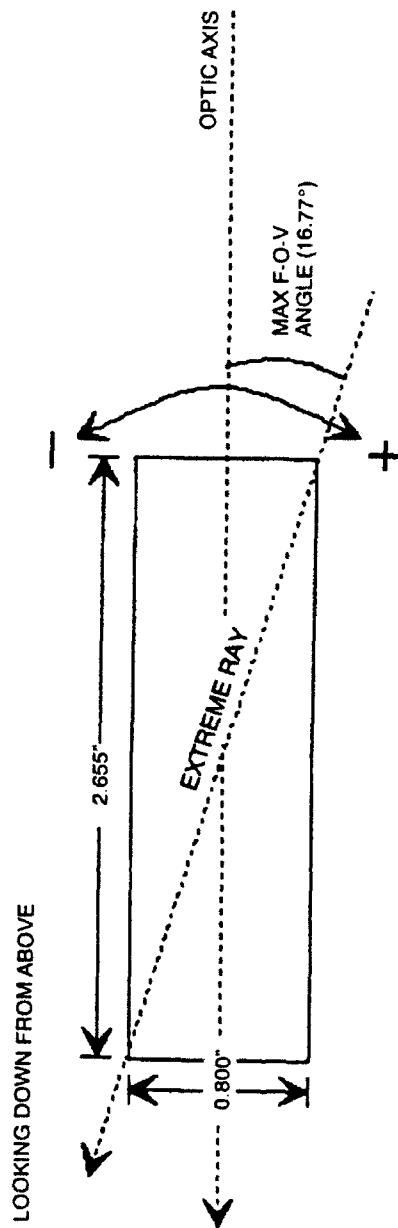


Figure 22. Field-of-view angle, defining geometry.

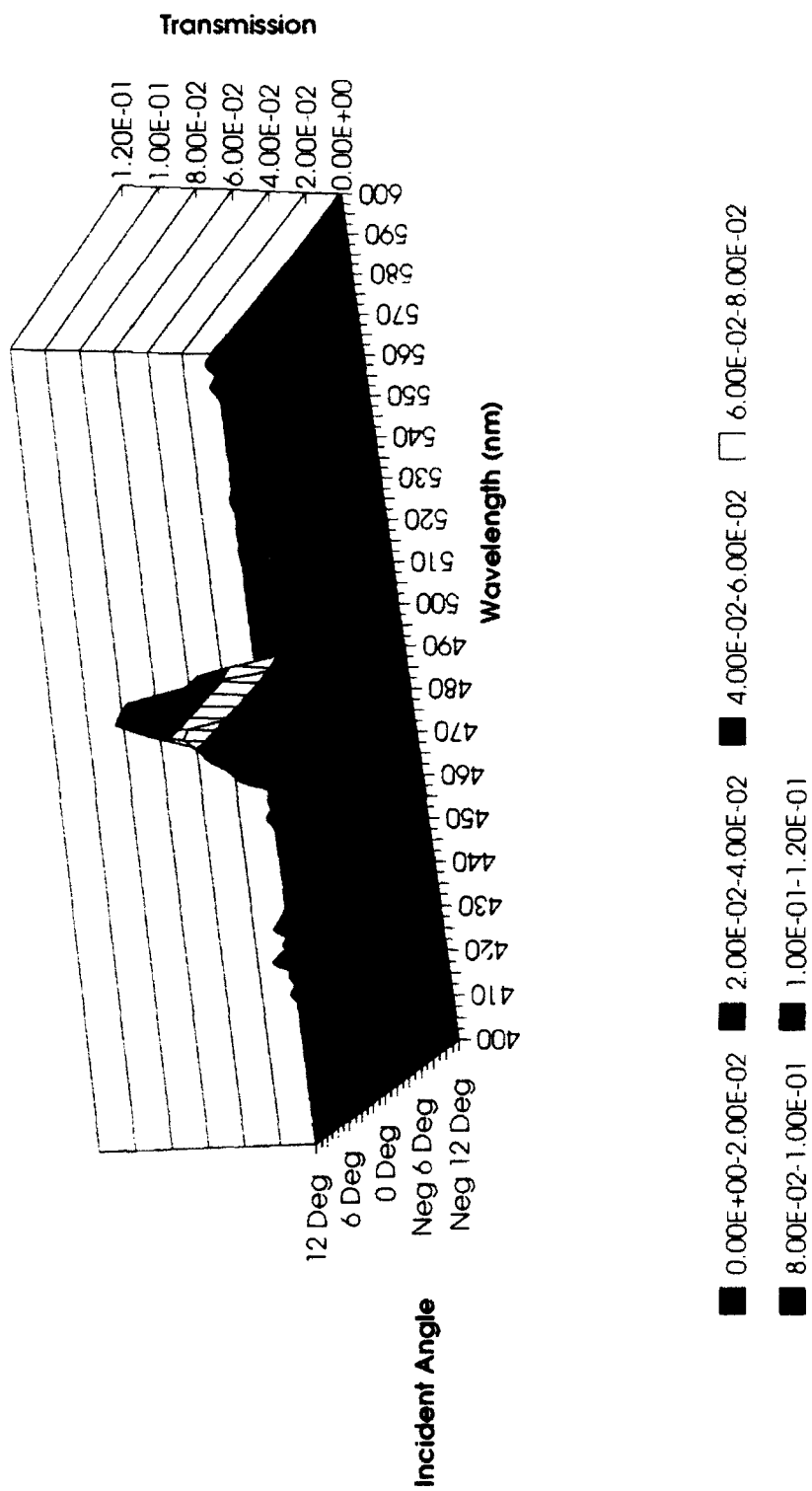


Figure 23. Transmission vs wavelength and incident angle (3-dimensional plot).

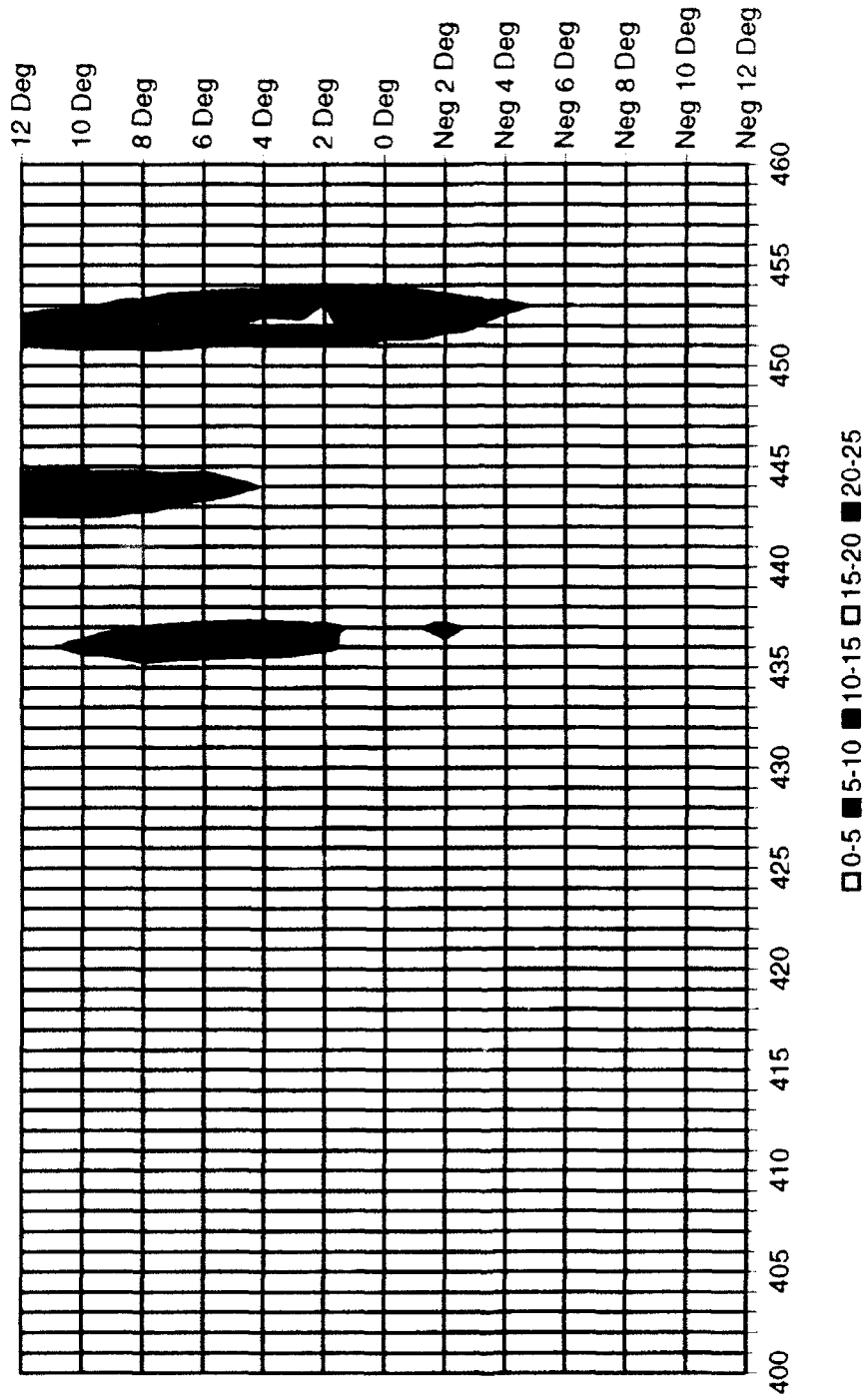


Figure 24. Transmission vs wavelength and incident angle (contour plot 400 λ <math><460</math>).

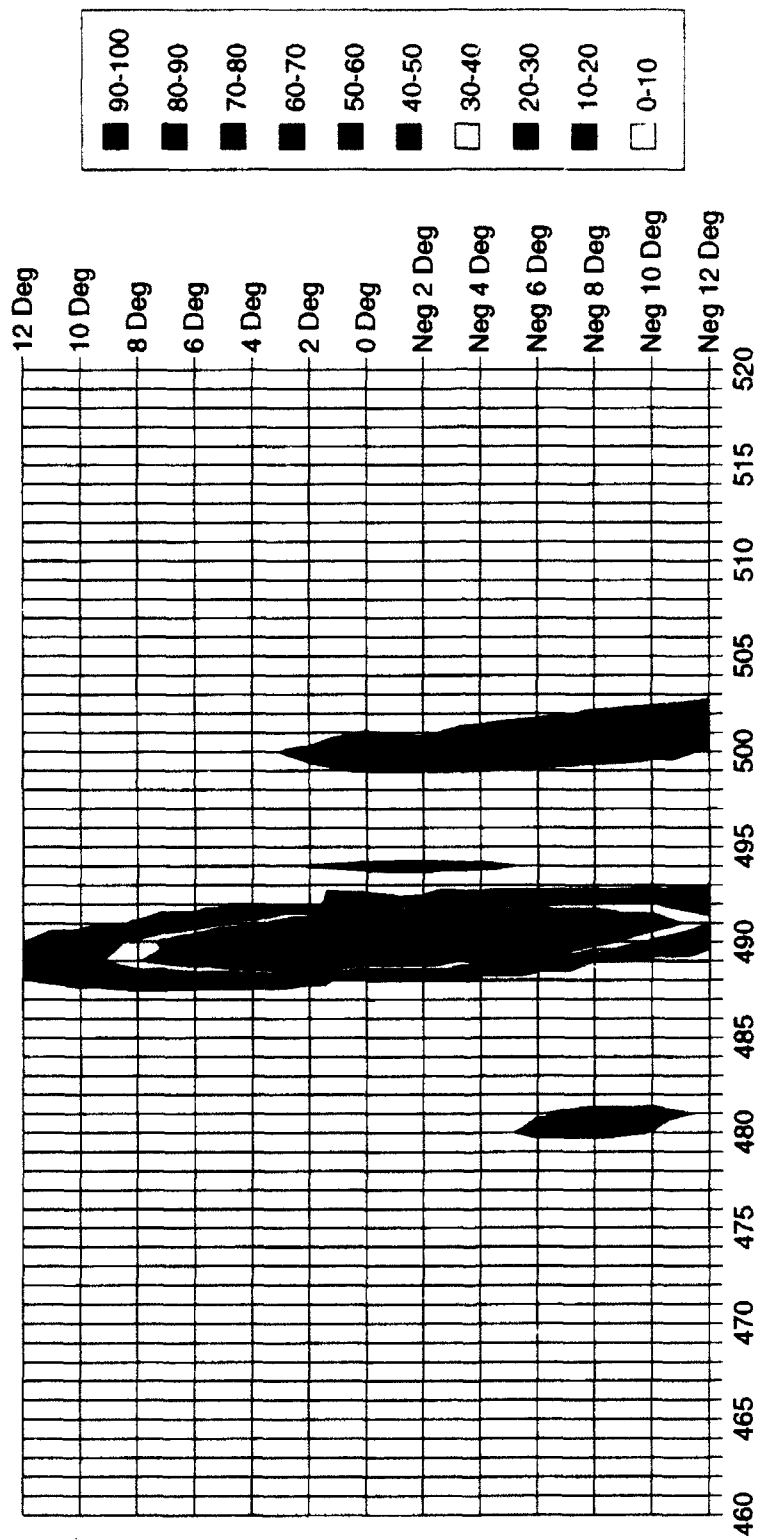


Figure 25. Transmissica vs wavelength and incident angle (contour plot 460 λ <math><520</math>).

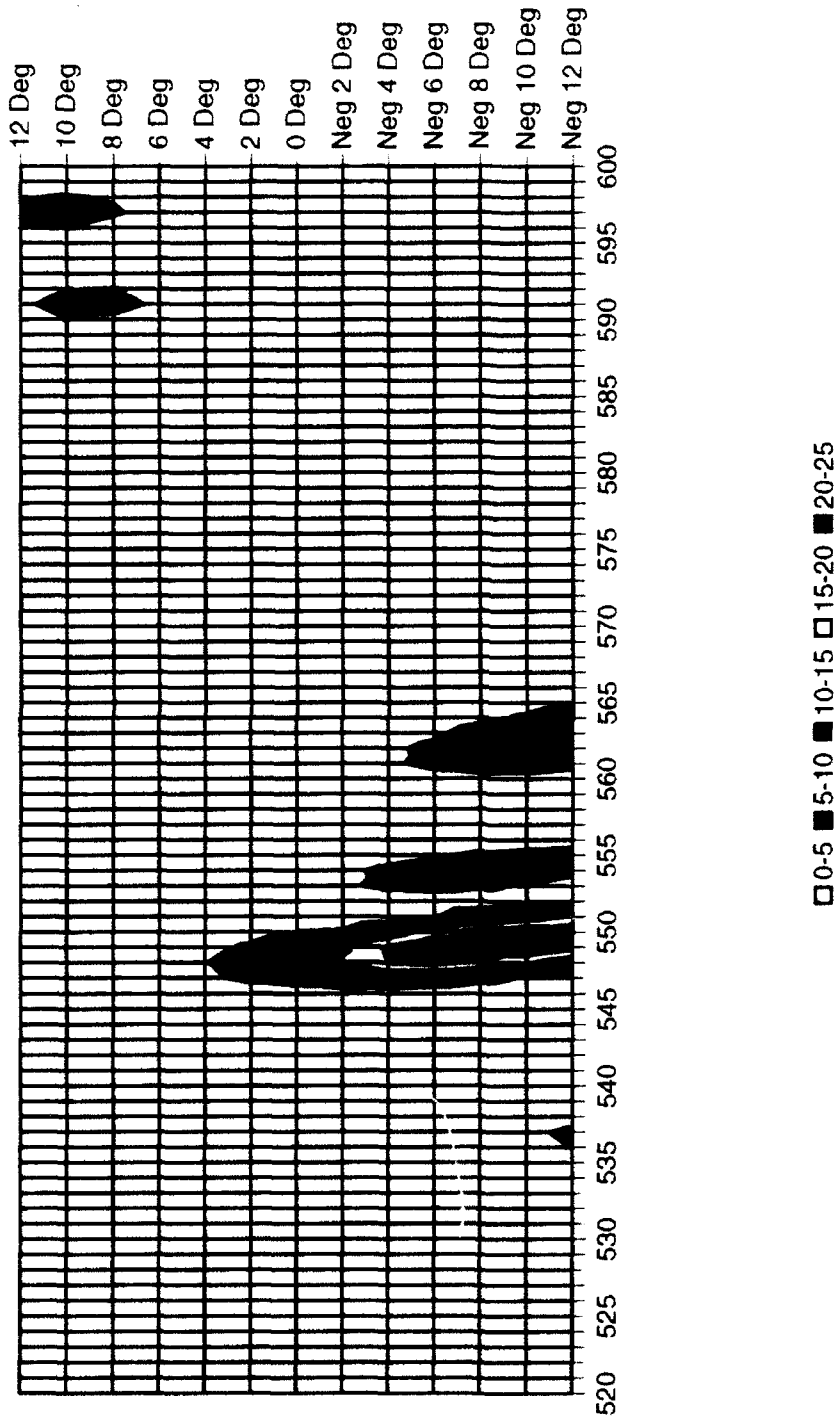


Figure 26. Transmission vs wavelength and incident angle (contour plot 520 λ <math><600</math>).

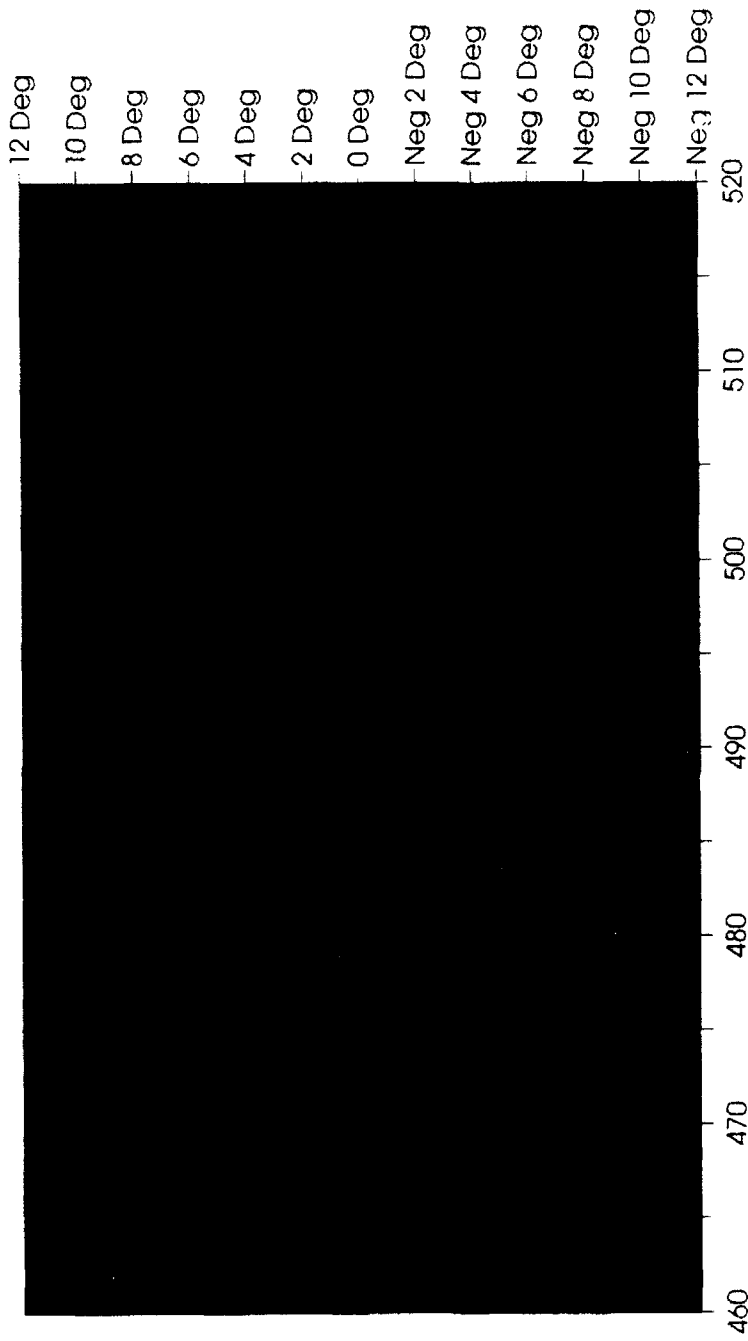


Figure 27. Transmission vs wavelength and incident angle (50% transmission contour).

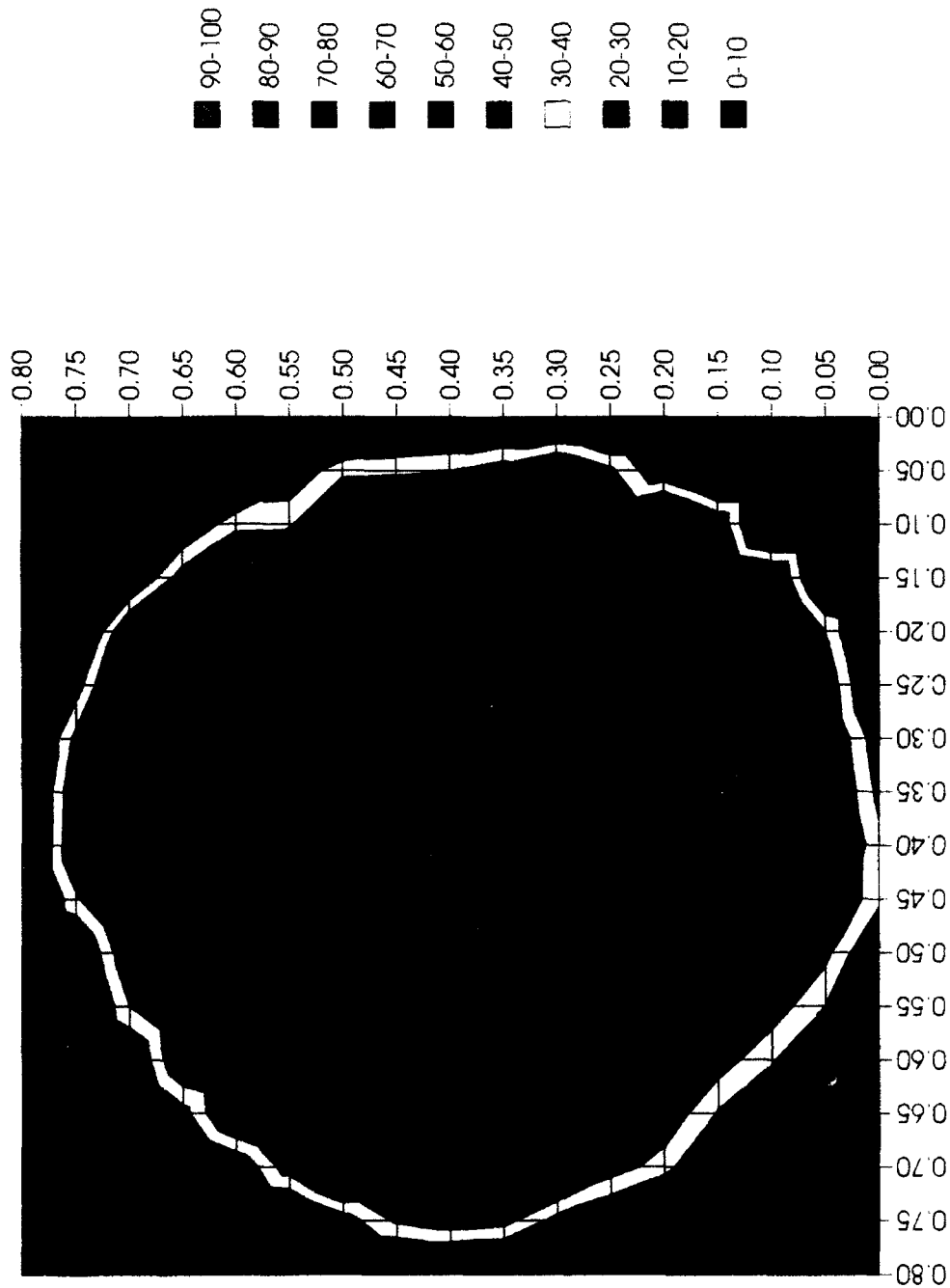


Figure 28. Normalized transmission uniformity contour plot.

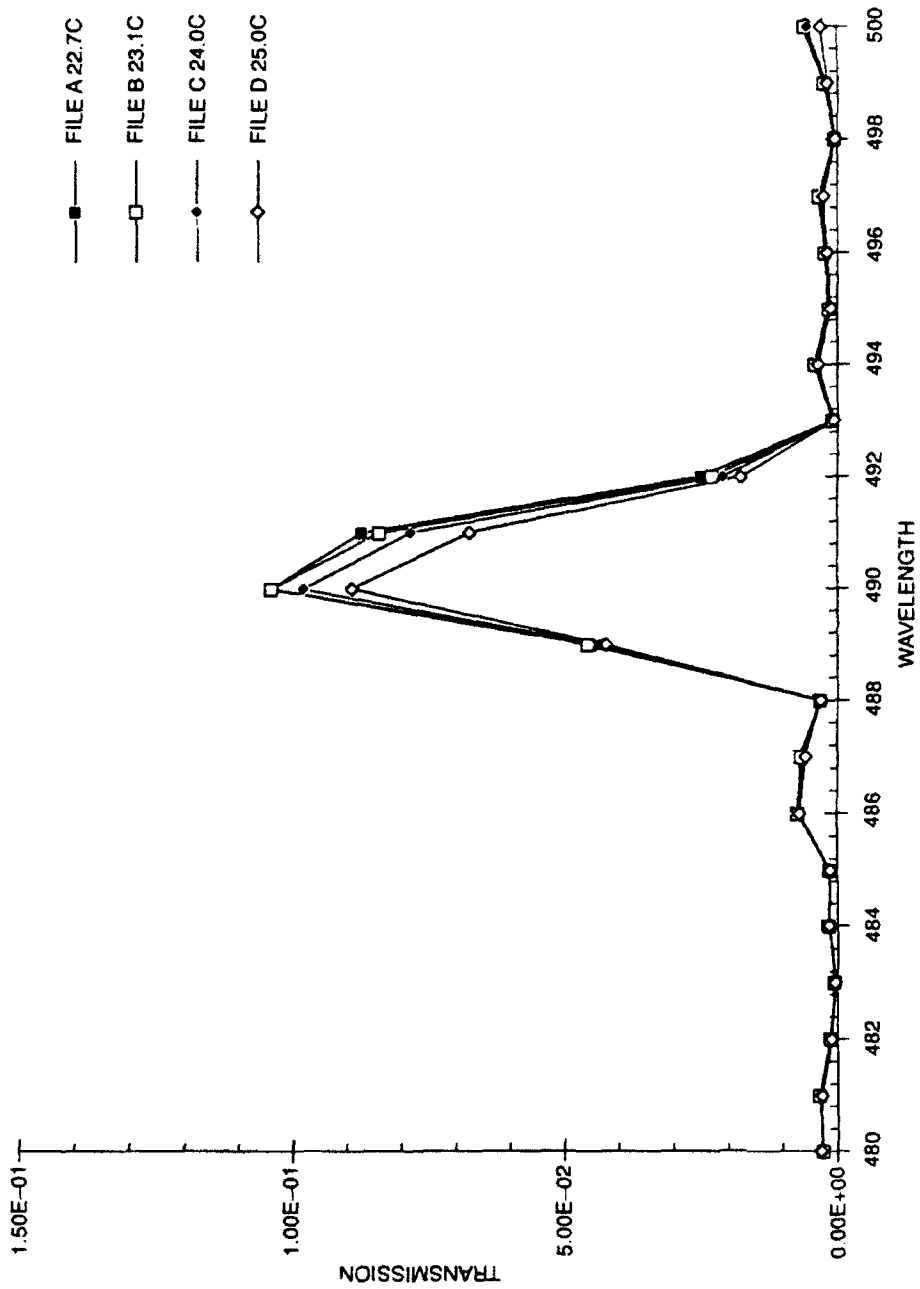


Figure 29. Transmission vs wavelength as temperature varies (filter set at 490 nm).

APPENDIX A
MEADOWLARK MODEL

This model was originally written at Meadowlark as a Mathcad document to assist in the design of the filter. Since its delivery to NRaD, it had been modified for use as a predictive tool to study the line width and out-of-band rejection of the filter. The model is incomplete in that it does not deal with the less than perfect transmission of the Polaroid dichroic sheet polarizers used in the design or the indium-tin oxide transparent electrodes used on the liquid crystal celis.

The following is a printout of the Mathcad document originally delivered by Meadowlark.

Six Element Lyot Filter Modeling Final Design

Input the desired wavelength range:	$\lambda := 410, 411.. 560$
Birefringent dispersion of Quartz:	$dnq(\lambda) := .0092 - \frac{.4956}{\lambda} + \frac{256.43}{\lambda^2}$
Birefringent dispersion of pn1 (20 C):	$dnpn1(\lambda) := .0007607 + \frac{.27753}{\lambda} - \frac{105.49}{\lambda^2}$
Birefringent dispersion of 2244 (20 C) LC1:	$dn2244(\lambda) := .0674 + \frac{2201}{\lambda^2}$
Cauchy fit for birefringent dispersion of 2140 (20 C) -LC2:	$n2140(\lambda) := .1071 + \frac{8048}{\lambda^2}$
Fit for 3 mil p2:	$R3p2(\lambda) := 2578.4 + \frac{.246111 \cdot 10^6}{\lambda} + \frac{0.1297 \cdot 10^9}{\lambda^2}$
Retardance of first element(waves):	$k := 2.5$
Retardance of negative polymer:	$p := 330$
Basic Liquid Crystal thickness at 490:	$t1 := \frac{k \cdot 560 - p}{dn2244(560)} \quad t1 = 1.438 \cdot 10^4$
Thickness of negative polymer:	$tp3 := 158750 \cdot \frac{p}{145}$

Operating wavelength: $w := 490$ $tun := 191$

Change these two numbers to watch the filter tune

First Element

$$A(\lambda) := \sin \left[\frac{\pi}{\lambda} \left[t1 \cdot dn2244(\lambda) + \left(tp3 \cdot dnpn1(\lambda) - \frac{tun}{dn2244(560)} \cdot dn2244(\lambda) \right) \right] \right]^2$$

Second Element

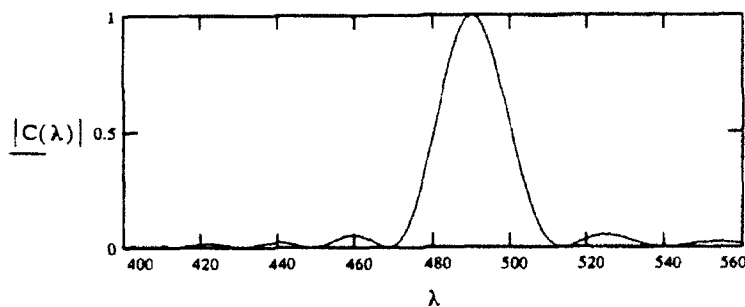
$$B(\lambda) := \cos \left[\frac{\pi}{\lambda} \cdot 2 \cdot \left[t1 \cdot dn2244(\lambda) + \left(tp3 \cdot dnpn1(\lambda) - \frac{tun}{dn2244(560)} \cdot dn2244(\lambda) \right) \right] \right]^2 \cdot A(\lambda)$$

Third Element

$$C(\lambda) := \cos \left[\frac{\pi}{\lambda} \cdot 4 \cdot 1 \cdot \left[t1 \cdot dn2244(\lambda) + \left(tp3 \cdot dnpn1(\lambda) - \frac{tun}{dn2244(560)} \cdot dn2244(\lambda) \right) \right] \right]^2 \cdot B(\lambda)$$

$$C(w) = 1$$

The first three stages are designed to be identical interger multiples in retardance. The materials used are a low dispersive liquid crystal (EM Chem.2244) and a negatively dispersive polymer to obtain a sufficient free spectral range Dispersion, rather than being used to describe the change in index is used here to describe the change of birefringence with wavelength. As voltage is applied to the liquid crystal, the retardance of the stages decreases. We follow the same wave from 560 to 420 in order to suppress the out-of-band.

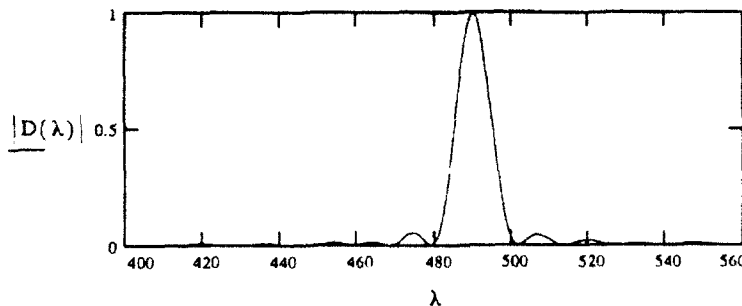


The fourth stage is made of a combination of polymers and a more dispersive liquid crystal. These materials are oriented with their fast axis opposing. This allows us to use the dispersion of the polymers to our benefit; in fact, we are able to substitute dispersion for retardance. If we tune wisely, we can suppress the out-of-band transmission by choosing how much retardance to place on the LC. For example, if the stage tunes to the correct wavelength when the retardance of the LC is set to x nm, it will also tune to that wavelength at about x+ w nm. One of these cases will more closely match the necessary FWHM to accommodate the other stages and minimize the leaks. If the entire filter were designed with similar polymers, the dispersions would match and it would be much easier to calibrate the filter. We hope to be able to investigate this more in the future.

Fourth Element

$$tun := 490$$

$$D(\lambda) := \cos \left[\frac{\pi}{\lambda} \left[2 \cdot R3p2(\lambda) + 1 \cdot tp3 \cdot dnpn1(\lambda) + 800 - \left(\left(\frac{tun}{n2140(560)} \cdot n2140(\lambda) \right) \right) \right] \right]^2 \cdot C(\lambda)$$



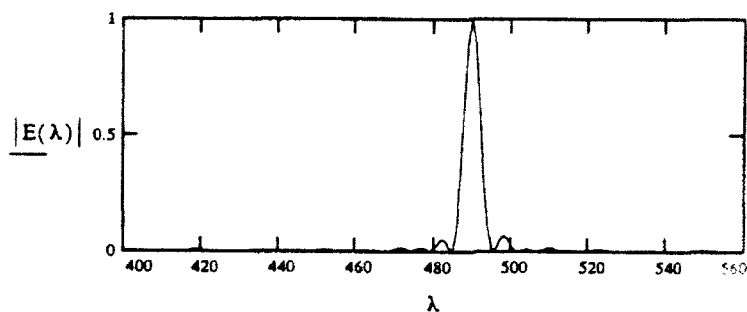
$$D(w) = 0.999$$

The fifth and sixth elements consist of quartz, wide field achromatic half wave retarders and a highly dispersive liquid crystal for tuning. As the LC is crossed with the axis of the adjacent quartz window, we can use the dispersion in our favor. This is not unlike designing an achromatic waveplate.

Fifth Element

$$tun := 610$$

$$E(\lambda) := \cos \left[\frac{\pi}{\lambda} \left(2 \cdot 1120000 \cdot dnq(\lambda) - \frac{tun}{n2140(560)} \cdot n2140(\lambda) \right) \right]^2 \cdot D(\lambda) \quad E(w) = 0.999$$



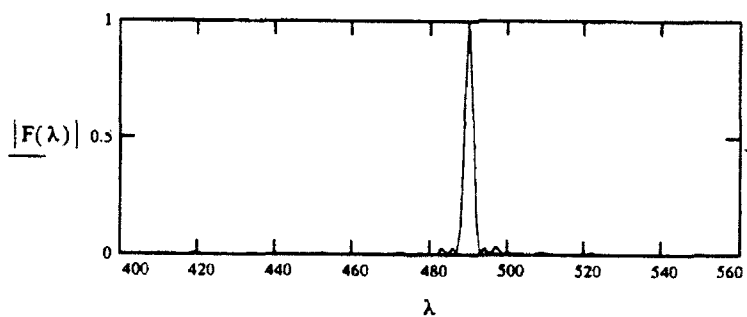
of waves at 560 (40)

$$\frac{1120000 \cdot 2 \cdot dnq(560)}{560} = 36.531$$

Sixth Element

$$tun := 290$$

$$F(\lambda) := \cos \left[\frac{\pi}{\lambda} \left(4 \cdot 1120000 \cdot dnq(w) - \frac{tun}{n2140(560)} \cdot n2140(\lambda) \right) \right]^2 \cdot E(\lambda) \quad F(w) = 0.999$$

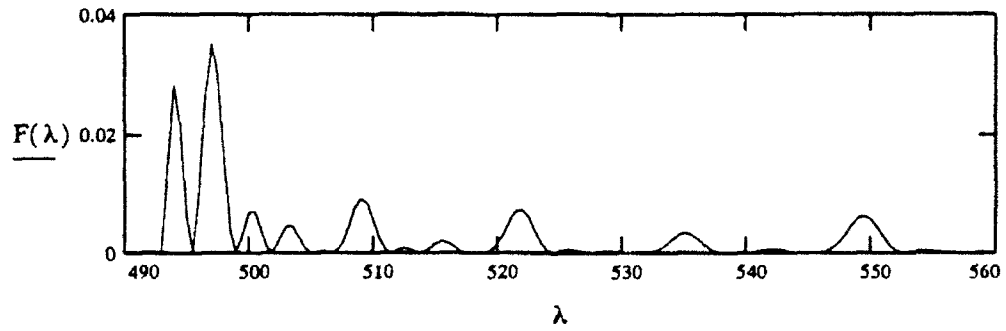


FWHM est.

$$\frac{w^2 \cdot .88}{2 \cdot 4 \cdot 1120000 \cdot dnq(w)} = 2.548$$

Detail of out-of-band rejection

$$\lambda := w + 3, w + 3.5 \dots 556$$



$$P := \frac{\int_{420}^{w-3} F(\lambda) d\lambda + \int_{w+3}^{560} F(\lambda) d\lambda}{\int_{w-3}^{w+3} F(\lambda) d\lambda}$$

% of power in out of band

$$P = 0.139$$

Rejection/nm

$$\frac{P}{560 - 420} = 9.925 \cdot 10^{-4}$$

APPENDIX B

EQUIPMENT LIST AND PROCEDURES

Spectral and field-of-view measurements.

Equipment	Manufacturer	Model	Serial No.
Monochromator	Optronics	740-A	85264-D
Radiometer	Optronics	730	850205
Wavelength Controller	Optronics	740-1C	85085
Collimating Lens	Optronics	740-72	9120092
Photo Detector	Optronics	730-5C	828
Lamp and Power Supply	Oriel	68735	518

The equipment was set up as shown in figure B-1 for the spectral and field-of-view measurements. For the field-of-view measurements, the filter was mounted on a calibrated turntable and rotated with respect to the axis of the output of the monochromator. The Hewlett-Packard computer controls the monochromator and collects data from the silicon photodiode by way of the Optronics radiometer. The computer uses a heavily modified version of a program that was originally provided with the monochromator to measure the spectral response of filters.

The data collected by the program reflects the absolute transmission of the filter. The program compensates for both the spectral transmission of the monochromator system and the spectral response of the detector by performing a calibration run prior to taking data on the filter under test. The data collected by the system is stored in the Hewlett-Packard binary format (BIN files) on a 5 1/4-inch floppy diskette. These files are later translated into ASCII data appropriate for use on an IBM-compatible computer using a commercial translation program from Oswego Corporation. These ASCII files are analyzed with a variety of IBM-compatible programs including Microsoft Excel, and Mathcad by Mathsoft.

Uniformity measurements.

Equipment	Manufacturer	Model	Serial No.
Rotation Stage	Newport	RSX-1	N/A
Translation Stage	Newport	420 & 430	N/A
Laser	Adlas	DPY-115C	H901002 & P901002
Radiometer	UDT	S390	1047

The set up for the uniformity measurements is shown in figure B-2. The laser is aligned so it strikes the front surface of the filter at normal incidence. After passing through the filter, the beam impinges on a silicon photodiode. The signal is read by the UDT radiometer that performs the ratio calculation between the throughput signal and the beam monitor signal. This ensures that fluctuations in the laser power do not effect the transmission data.

The filter is mounted on a pair of translation stages so it can be moved perpendicular to the beam in both directions independently. This permits the entire clear aperture of the filter to be addressed. The filter was moved manually using the micrometers on the translation stage. The raw data was recorded by hand and analyzed with Microsoft Excel. The data was normalized to the maximum transmission value, then plotted as a contour plot (figure 28).

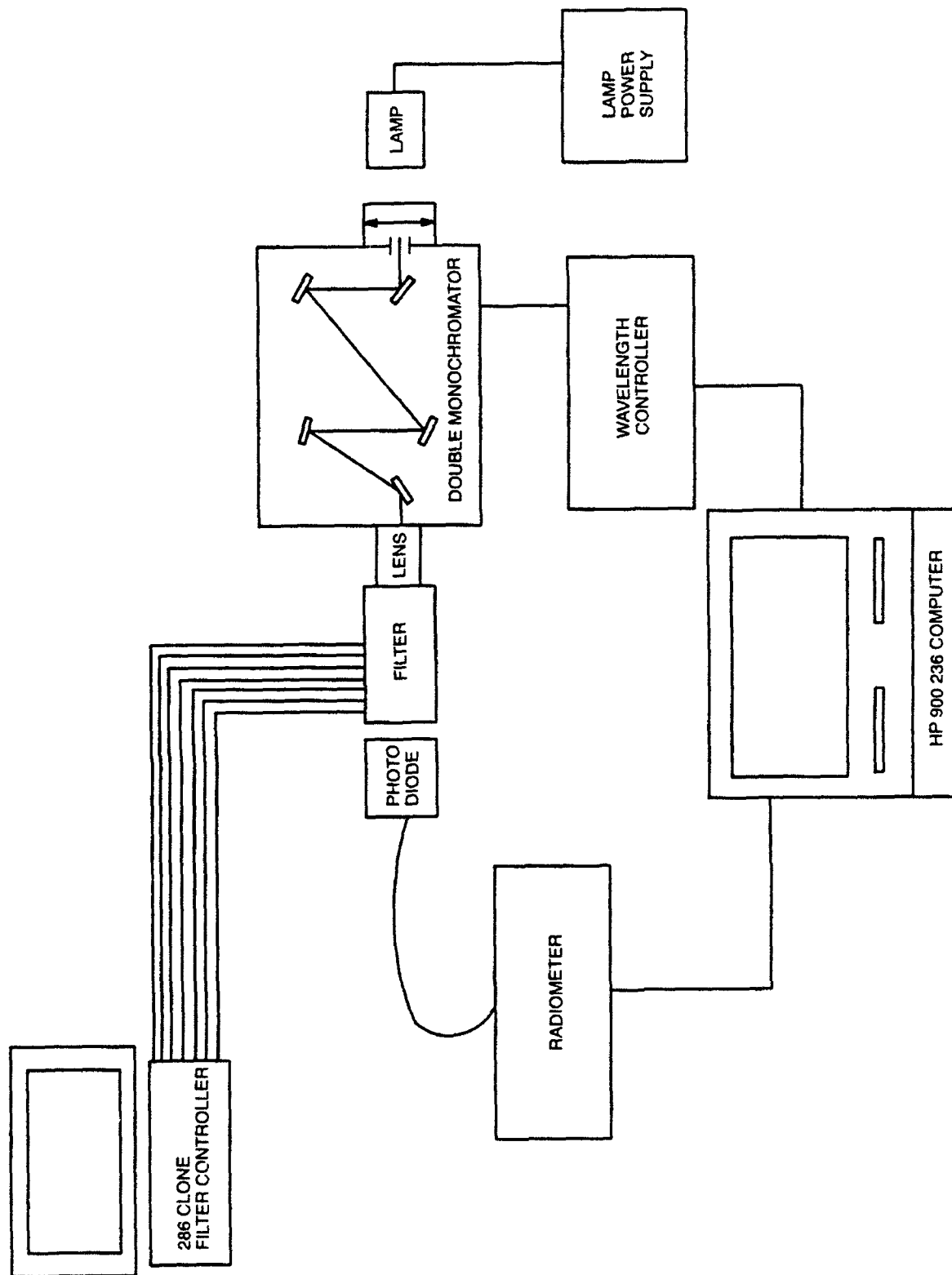


Figure B-1. Spectral measurement setup.

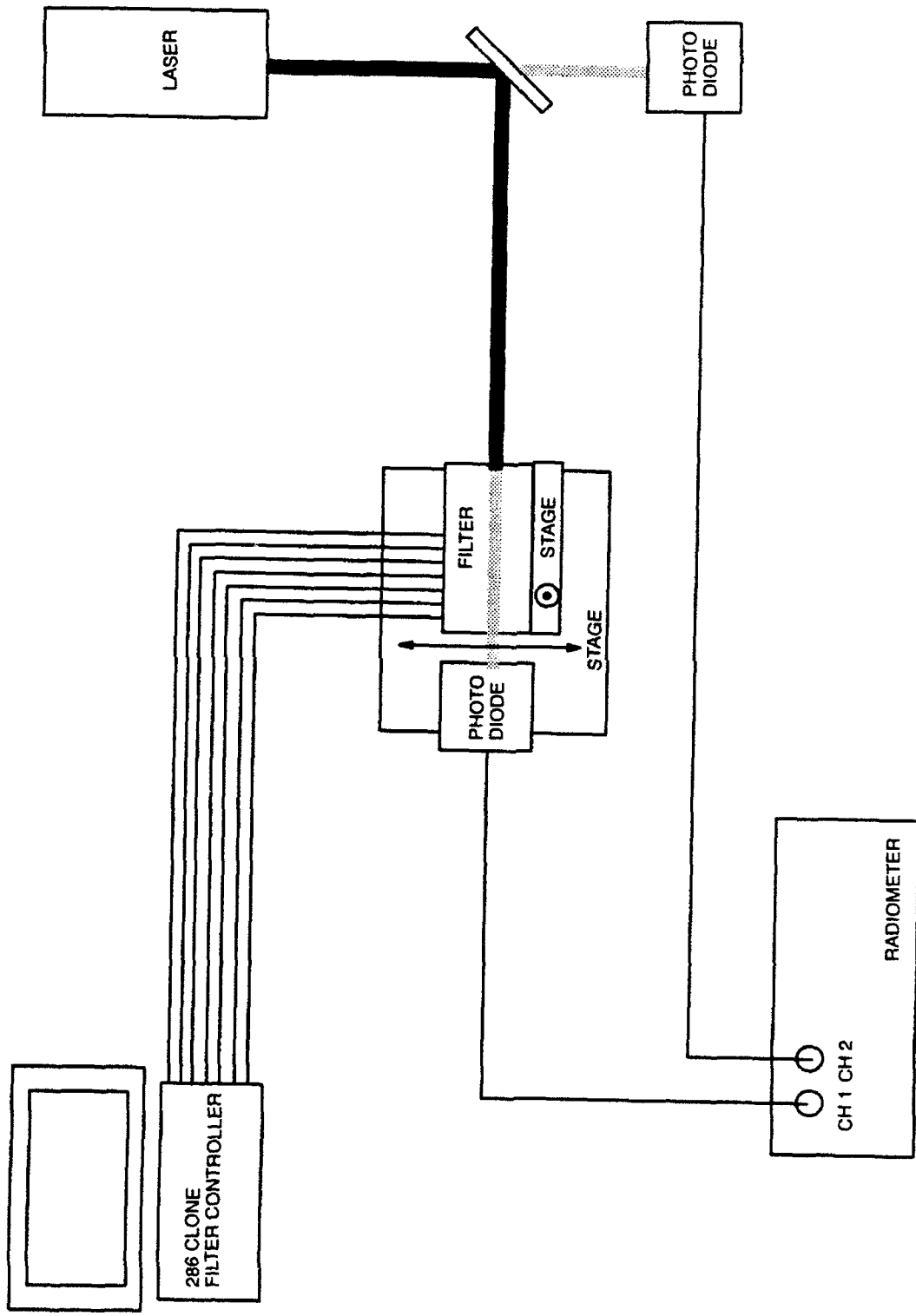


Figure B-2. Transmission uniformity setup.

APPENDIX C

**PEAK WAVELENGTH VS VOLTAGE DATA PROVIDED BY
MEADOWLARK**

The following tables contain the values of voltage (in millivolts) that must be placed on the liquid crystal variable retarders of each element in order to have a peak in the elements transmission spectrum at the specified wavelength. These values are stored in a file (filename: `filter.dat`) and loaded with the software for use by the control program. Note that the values for element #2 are the original values sent by Meadowlark, and are no longer valid after the element was repaired. The new values for element #2 are given in appendix D. In addition to the table, the values are also plotted in figures C-1 through C-6.

Wavelength	Voltages (millivolts)					
	Element #1	Element #2	Element #3	Element #4	Element #5	Element #6
420	4050	5375	4425	2781	2830	2763
421	4031	5363	4394	2890	2991	3507
422	4013	5352	4364	2985	3111	5768
423	3997	5342	4334	3093	3189	2543
424	3984	5333	4304	3283	3394	2993
425	3975	5325	4275	3413	3517	4082
426	3970	5317	4245	3617	3726	7466
427	3969	5310	4218	3813	3880	2598
428	3970	5302	4192	4093	4172	3189
429	3972	5290	4169	4497	3003	4586
430	3975	5275	4150	4850	3129	7361
431	3976	5253	4134	2500	3242	2720
432	3976	5228	4121	2573	3371	3407
433	3976	5201	4108	2605	3547	4402
434	3975	5174	4093	2709	3709	9431
435	3975	5150	4075	2800	3910	2714
436	3974	5128	4050	2890	4092	3324
437	3974	5108	4022	2961	4446	4353
438	3974	5086	3990	3118	3063	8745
439	3974	5059	3957	3212	3194	2708
440	3975	5025	3925	3336	3324	3430
441	3975	4980	3893	3560	3517	4669
442	3976	4932	3864	3640	3657	9562
443	3976	4885	3839	2271	3870	2733
444	3976	4847	3817	2302	4048	3264
445	3975	4825	3800	2370	4414	4492
446	3972	4821	3787	2414	3021	9616

	Voltages (millivolts)					
Wavelength	Element #1	Element #2	Element #3	Element #4	Element #5	Element #6
447	3968	4833	3778	2481	3159	2611
448	3963	4850	3770	2494	3253	3171
449	3957	4867	3761	2573	3406	3883
450	3950	4875	3750	2641	3528	7491
451	3941	4868	3733	2732	3721	2544
452	3932	4850	3713	2784	3850	2926
453	3921	4825	3691	2876	4194	3593
454	3911	4798	3669	2962	4374	5810
455	3900	4775	3650	3081	4778	2408
456	3888	4757	3633	3134	5008	2696
457	3876	4746	3618	3283	5650	3218
458	3862	4738	3604	3395	6306	4735
459	3845	4732	3590	3553	7389	8995
460	3825	4725	3575	3767	8810	2527
461	3800	4715	3556	4031	3950	2992
462	3774	4704	3536	4296	4110	3991
463	3747	4693	3515	4541	4408	6317
464	3721	4683	3494	5062	4728	2401
465	3700	4675	3475	5456	5089	2787
466	3683	4669	3457	5919	5620	3483
467	3670	4665	3442	6898	6084	4481
468	3662	4662	3428	8108	7525	7701
469	3655	4657	3414	9010	8283	2475
470	3650	4650	3400	2641	11090	2854
471	3644	4638	3384	2720	3981	3553
472	3639	4623	3368	2781	4258	5036
473	3634	4607	3352	2860	4481	11582
474	3629	4590	3338	2908	4768	2592
475	3625	4575	3325	3004	5311	2902
476	3620	4561	3314	3111	5678	3617
477	3615	4550	3304	3218	6439	4890
478	3610	4541	3295	3302	7374	2271
479	3605	4533	3286	3459	9175	2518

	Voltages (millivolts)					
Wavelength	Element #1	Element #2	Element #3	Element #4	Element #5	Element #6
480	3600	4525	3275	3628	11540	3010
481	3594	4516	3261	3795	3966	3779
482	3589	4508	3246	3985	4262	5934
483	3584	4498	3230	4166	4447	2253
484	3579	4487	3214	4496	4920	2584
485	3575	4475	3200	4845	5165	2919
486	3570	4460	3187	5242	5565	3733
487	3565	4445	3176	5856	6516	5434
488	3560	4429	3167	6684	7014	2246
489	3555	4414	3158	7209	9008	2562
490	3550	4400	3150	8184	10400	2908
491	3544	4387	3141	2568	3887	3523
492	3539	4377	3132	2617	4098	5482
493	3534	4367	3122	2653	4340	10892
494	3529	4358	3111	2705	4713	2434
495	3525	4350	3100	2757	4894	2696
496	3520	4340	3086	2835	5277	3236
497	3515	4330	3072	2869	5992	4398
498	3510	4320	3056	2932	6504	6993
499	3505	4310	3041	3045	7775	2289
500	3500	4300	3025	3111	9125	2538
501	3494	4289	3009	3236	3714	2968
502	3489	4279	2993	3336	3950	3848
503	3484	4270	2978	3395	4081	5726
504	3479	4260	2963	3605	4347	2159
505	3475	4250	2950	3758	4614	2427
506	3470	4239	2937	3845	4795	2756
507	3465	4229	2925	4053	5412	3330
508	3460	4219	2915	4285	5715	4058
509	3455	4209	2906	4636	6464	8810
510	3450	4200	2900	4975	7624	2240
511	3444	4190	2895	5204	8831	2555
512	3439	4182	2892	5418	11053	2836

	Voltages (millivolts)					
Wavelength	Element #1	Element #2	Element #3	Element #4	Element #5	Element #6
513	3434	4172	2888	6053	3807	3553
514	3429	4162	2883	6934	3944	5040
515	3425	4150	2875	7775	4174	8724
516	3420	4136	2862	8557	4352	2278
517	3415	4120	2847	9377	4585	2537
518	3410	4104	2831	2482	5075	2938
519	3405	4089	2815	2555	5363	3668
520	3400	4075	2800	2598	5846	4916
521	3393	4062	2787	2631	6948	11980
522	3385	4051	2776	2708	7454	2333
523	3376	4041	2767	2751	9522	2519
524	3364	4032	2758	2818	11800	2973
525	3350	4025	2750	2859	3720	3583
526	3333	4018	2740	2943	3961	5290
527	3316	4012	2730	2991	4105	9635
528	3303	4006	2720	3069	4306	2302
529	3296	4002	2710	3165	4662	2475
530	3300	4000	2700	3247	4834	2763
531	3315	3998	2689	3324	5149	3471
532	3337	3996	2679	3413	5714	4498
533	3361	3992	2669	3489	6403	8435
534	3379	3986	2659	3680	7154	2197
535	3387	3975	2650	3807	8761	2414
536	3379	3958	2640	4002	10012	2659
537	3359	3938	2630	4076	3571	3111
538	3331	3916	2620	4357	3789	4007
539	3302	3894	2610	4608	3910	5600
540	3275	3875	2600	4845	4087	2040
541	3254	3859	2589	5192	4390	2302
542	3240	3847	2578	5410	4557	2531
543	3231	3838	2567	5699	4769	2908
544	3226	3830	2558	6516	5332	3483
545	3225	3825	2550	7194	5608	4762

	Voltages (millivolts)					
Wavelength	Element #1	Element #2	Element #3	Element #4	Element #5	Element #6
546	3225	3819	2543	8065	6059	7628
547	3227	3814	2538	8665	6988	2141
548	3228	3809	2534	2364	7962	2402
549	3228	3804	2530	2413	9256	2635
550	3225	3800	2525	2463	12228	3111
551	3218	3795	2518	2487	3692	3996
552	3208	3790	2510	2475	3789	5519
553	3197	3785	2501	2561	3967	11081
554	3185	3780	2489	2583	4200	2203
555	3175	3775	2475	2617	4341	2395
556	3165	3769	2458	2683	4553	2671
557	3157	3764	2439	2720	4910	3104
558	3151	3759	2418	2763	5220	3755
559	3145	3754	2397	2823	5693	5507
560	3140	3750	2375	2838	6449	11362

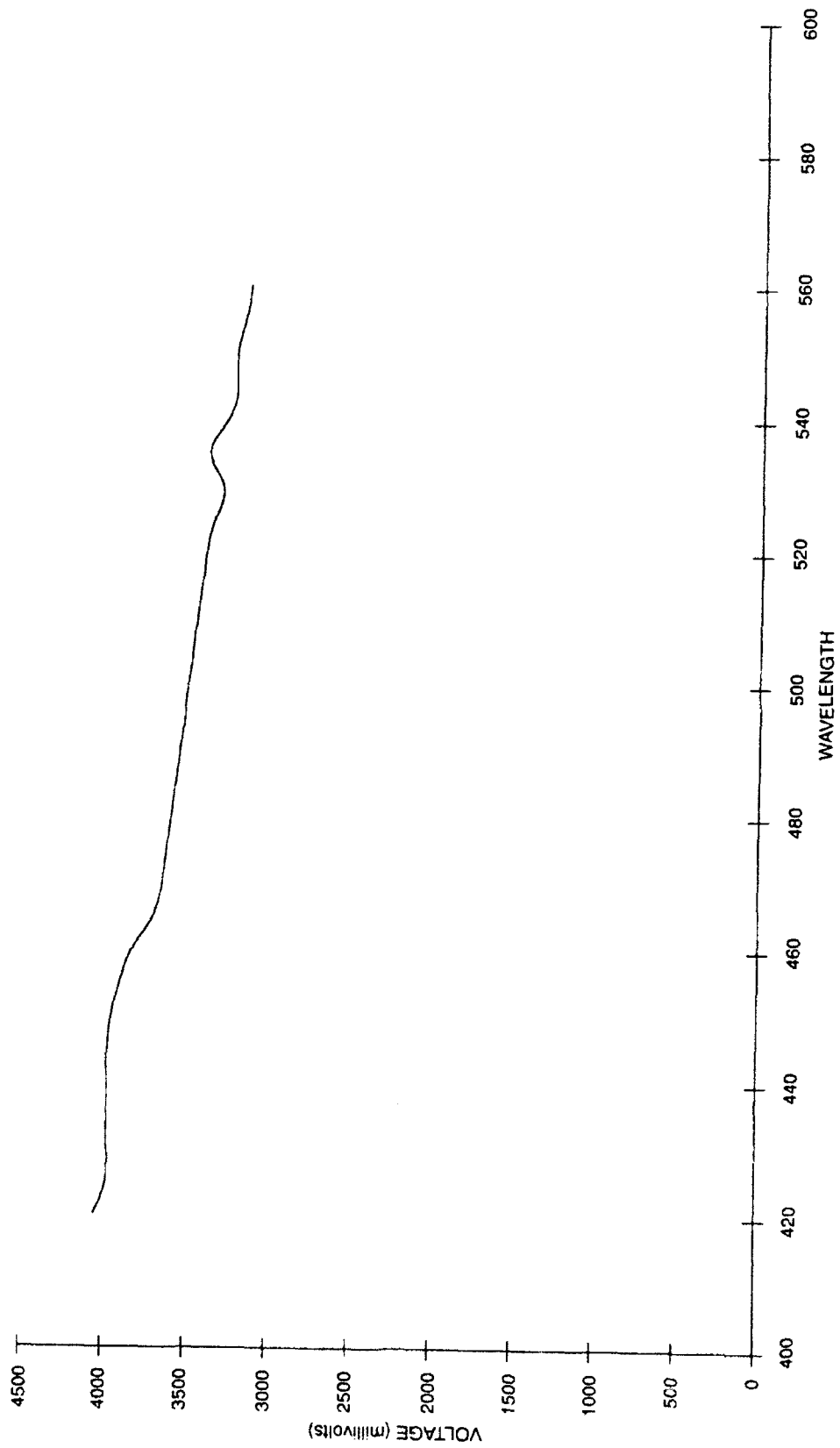


Figure C-1. Calibration voltage vs wavelength (element #1).

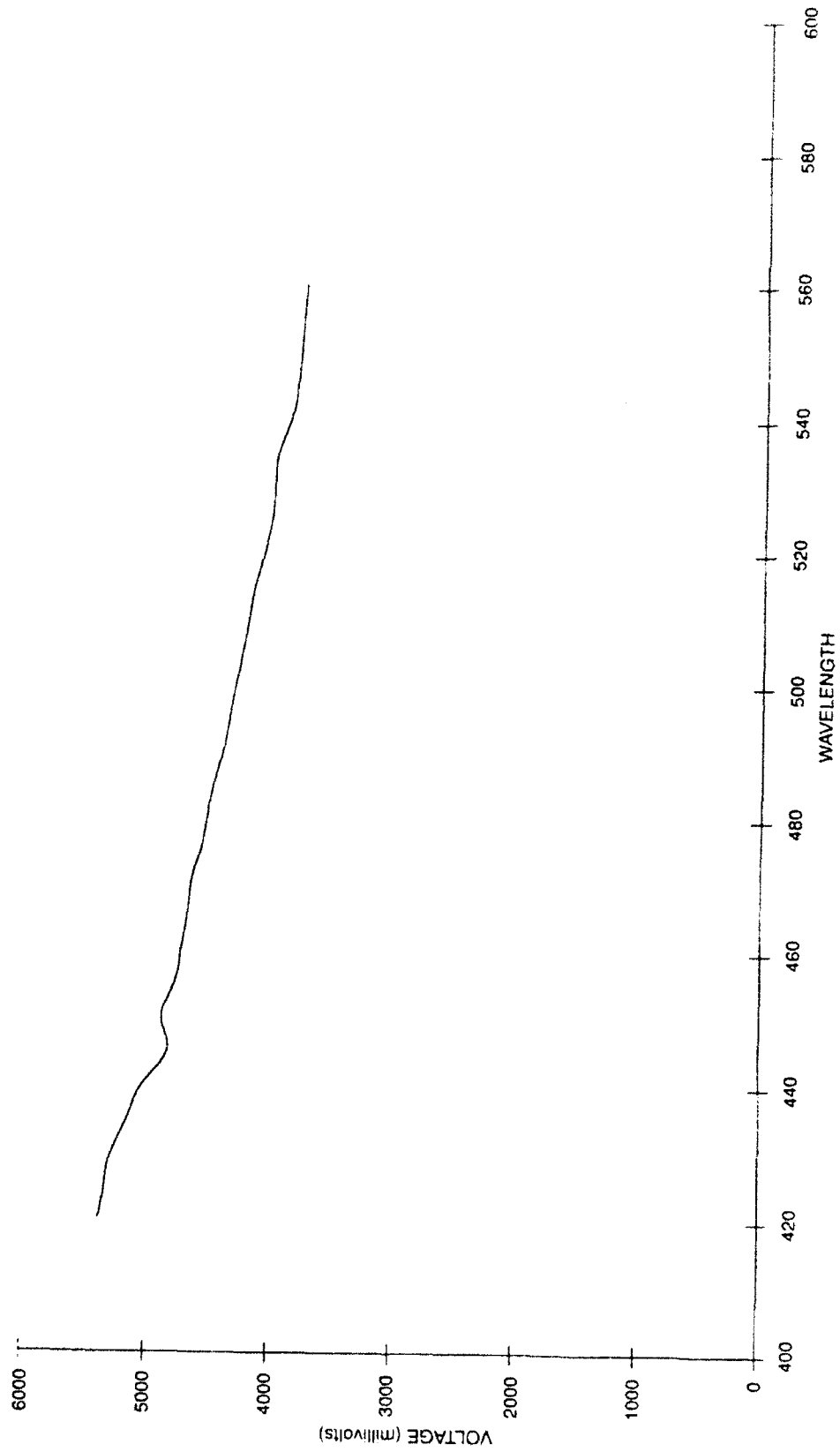


Figure C-2. Calibration voltage vs wavelength (element #2 as originally delivered).

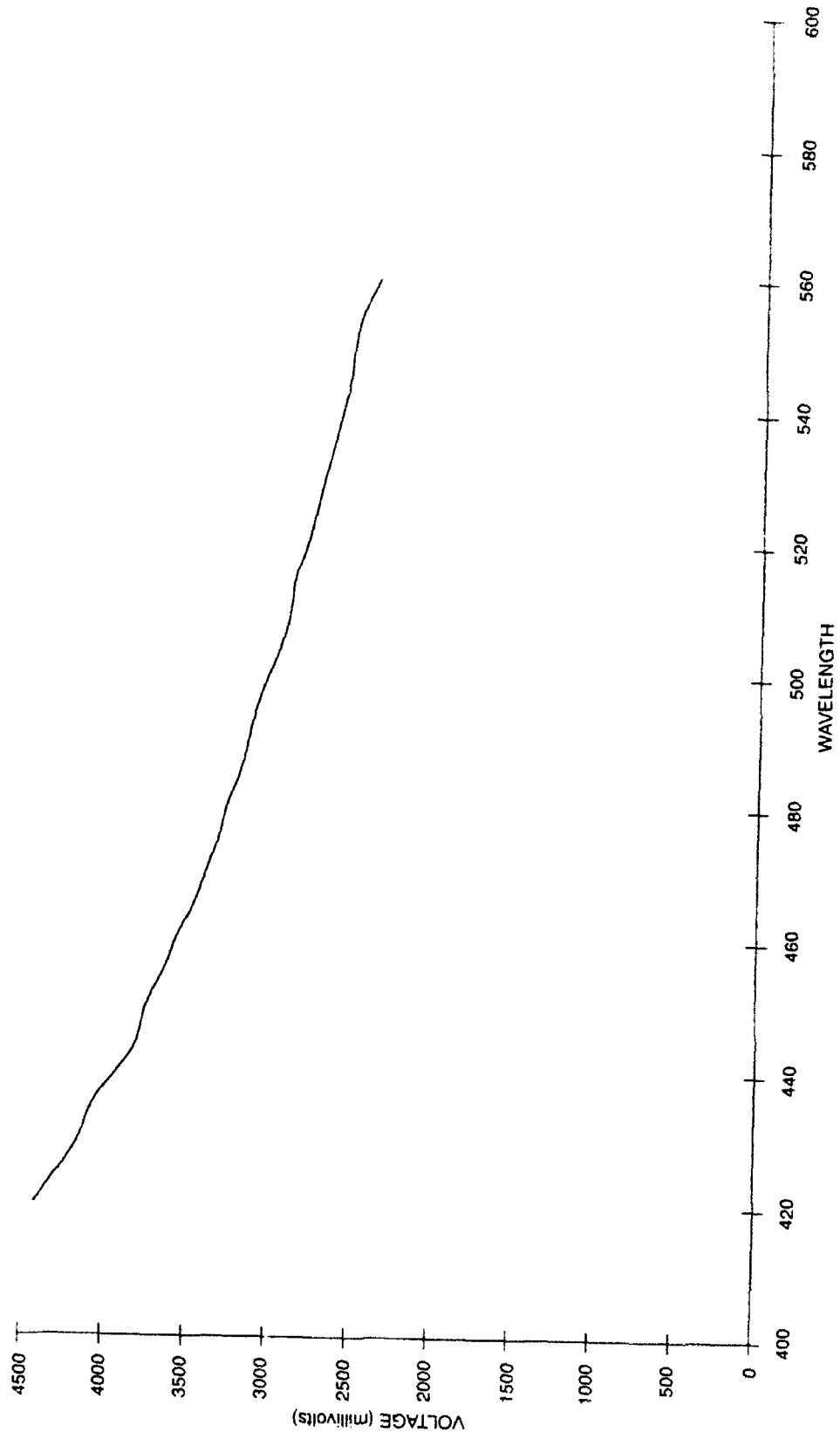


Figure C-3. Calibration voltage vs wavelength (element #3).

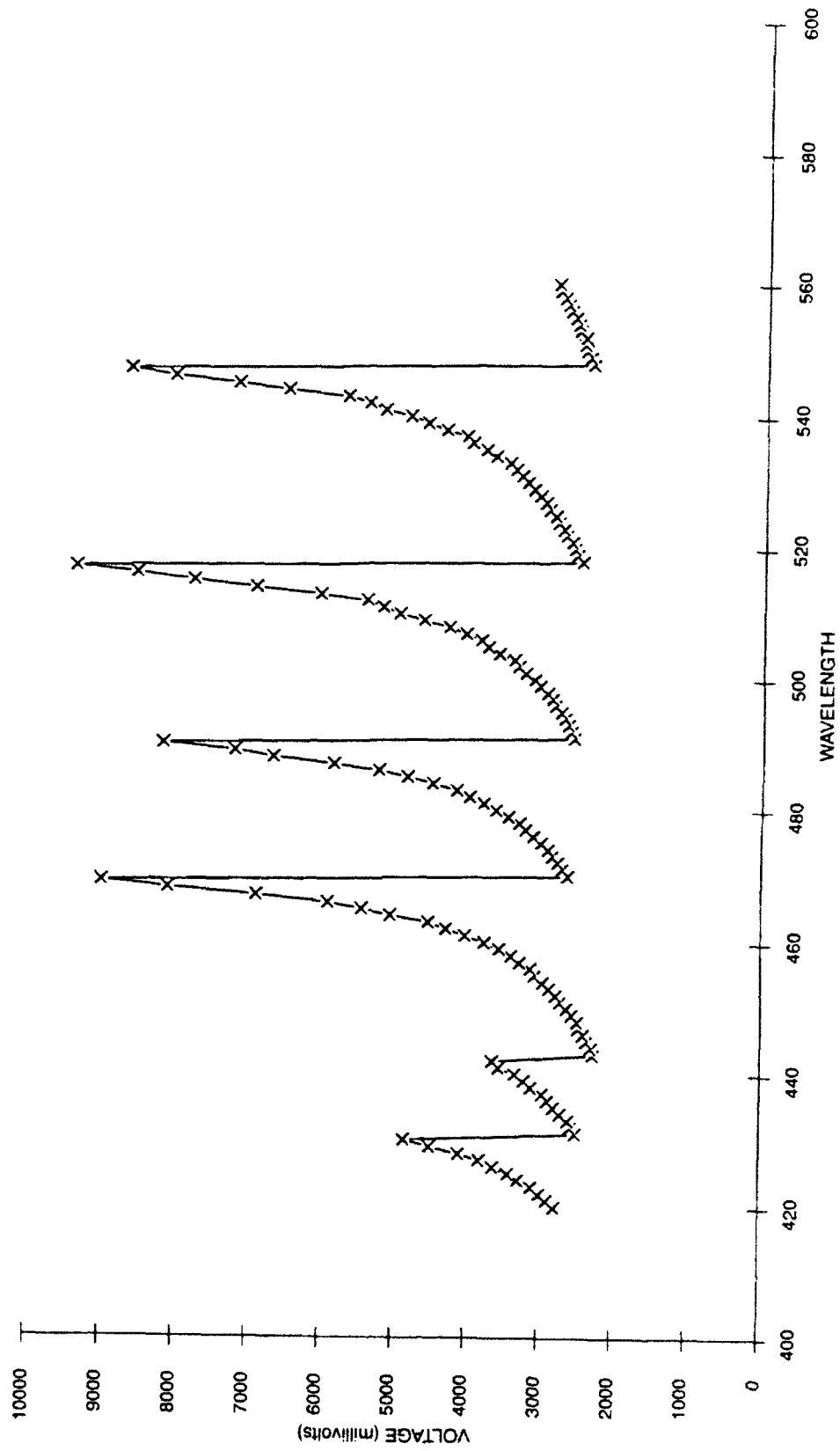


Figure C-4. Calibration voltage vs wavelength (element #4).

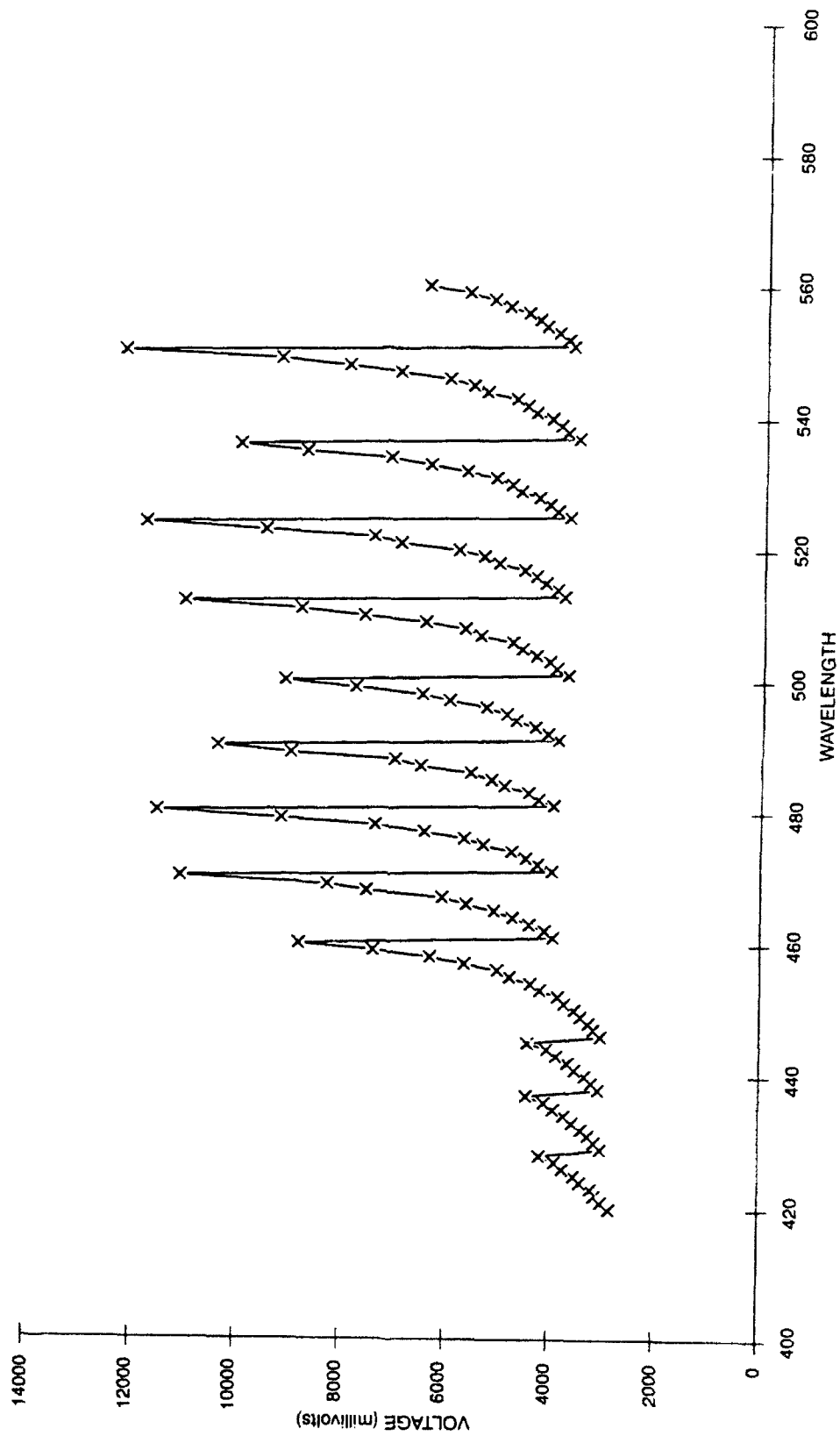


Figure C-5. Calibration voltage vs wavelength (element #5).

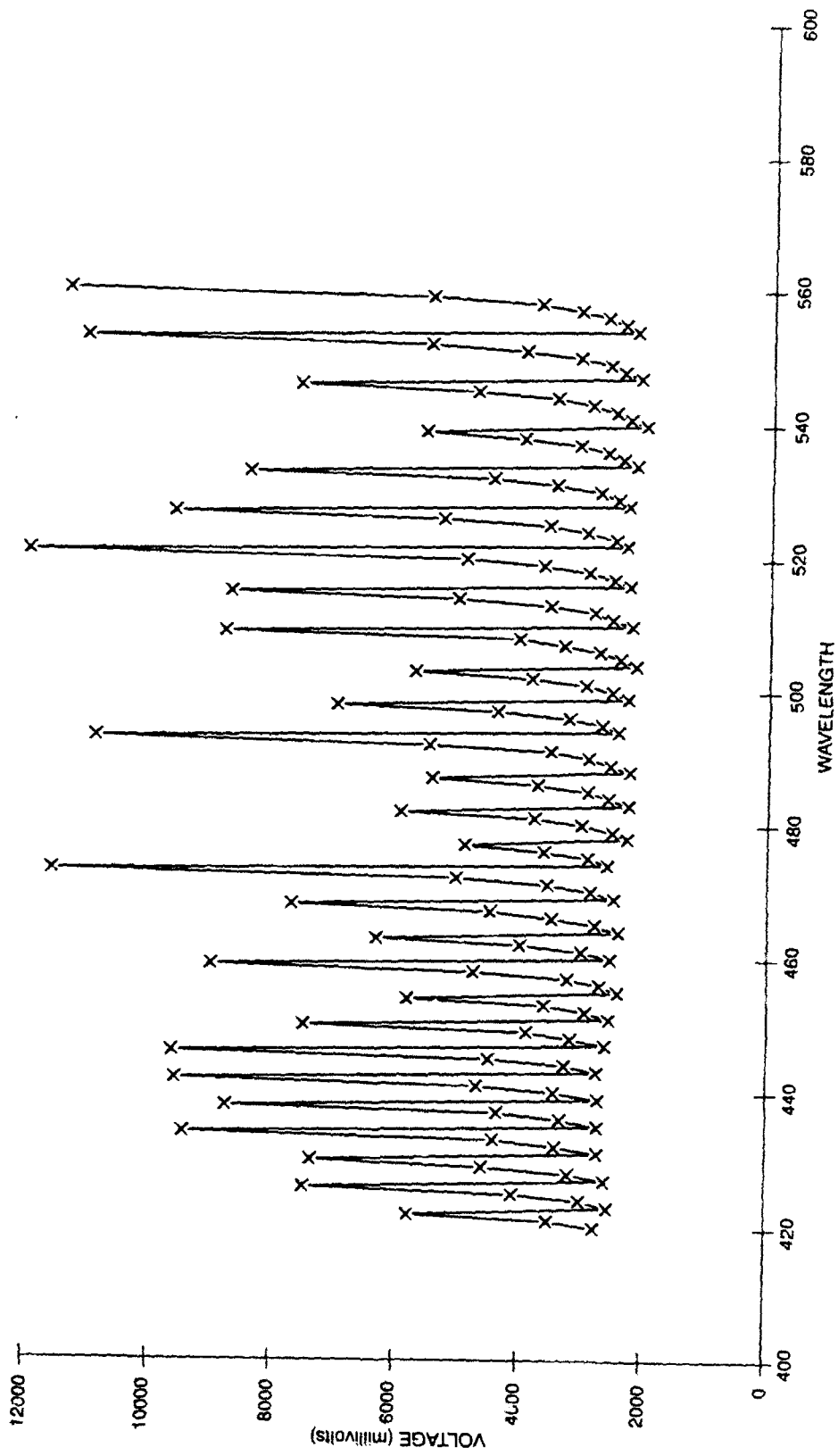


Figure C-6. Calibration voltage vs wavelength (element #6).

APPENDIX D

**PEAK WAVELENGTH VS VOLTAGE DATA PROVIDED BY NRaD FOR
ELEMENT #2**

Wavelength	Voltage	Wavelength	Voltage	Wavelength	Voltage	Wavelength	Voltage
420	3324	454	3081	488	2860	522	2673
421	3319	455	3073	489	2853	523	2668
422	3313	456	3065	490	2846	524	2662
423	3306	457	3057	491	2839	525	2657
424	3298	458	3049	492	2832	526	2652
425	3290	459	3041	493	2826	527	2648
426	3281	460	3033	494	2820	528	2643
427	3273	461	3025	495	2815	529	2638
428	3264	462	3018	496	2811	530	2632
429	3255	463	3011	497	2808	531	2524
430	3246	464	3004	498	2805	532	2616
431	3238	465	2998	499	2802	533	2607
432	3230	466	2992	500	2798	534	2598
433	3222	467	2986	501	2793	535	2590
434	3214	468	2980	502	2787	536	2583
435	3206	469	2973	503	2780	537	2577
436	3198	470	2967	504	2773	538	2571
437	3190	471	2960	505	2767	539	2566
438	3183	472	2953	506	2762	540	2561
439	3176	473	2946	507	2757	541	2555
440	3169	474	2939	508	2752	542	2550
441	3163	475	2933	509	2747	543	2543
442	3157	476	2927	510	2741	544	2537
443	3152	477	2921	511	2735	545	2530
444	3147	478	2916	512	2727	546	2523
445	3141	479	2911	513	2720	547	2516
446	3135	480	2906	514	2713	548	2509
447	3129	481	2901	515	2707	549	2502
448	3122	482	2896	516	2702	550	2495
449	3116	483	2891	517	2697	551	2489
450	3109	484	2886	518	2693	552	2482
451	3102	485	2880	519	2689	553	2476
452	3095	486	2874	520	2684	554	2468
453	3088	487	2867	521	2679	555	2460

Wavelength	Voltage	Wavelength	Voltage	Wavelength	Voltage	Wavelength	Voltage
556	2450	559	2409				
557	2439	560	2390				
558	2425						

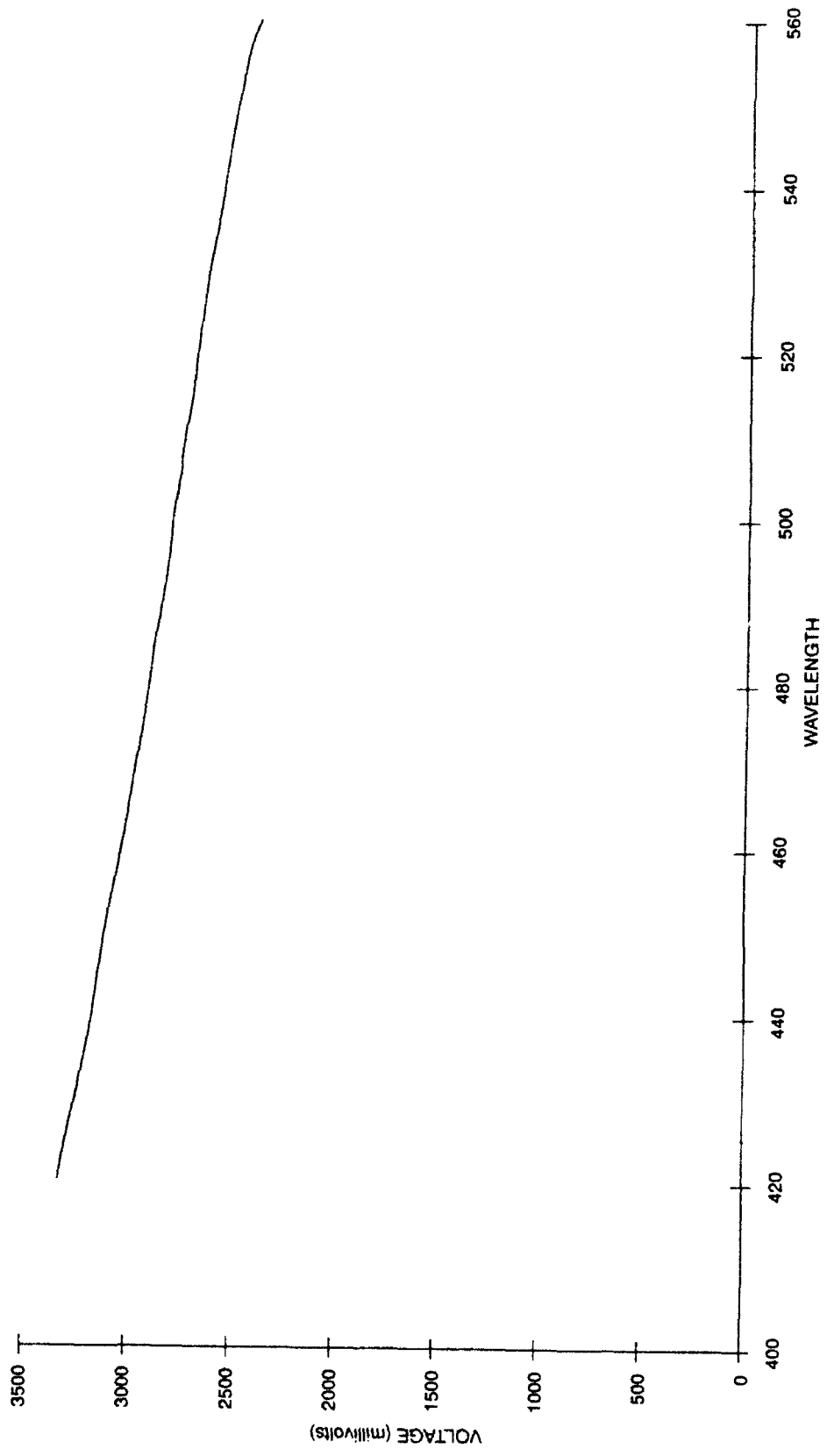


Figure D-1. Calibration voltage vs wavelength (element #2 as calibrated at NRaD).

APPENDIX E

FILTER RELIABILITY AND REPAIRS

FILTER RELIABILITY AND REPAIRS

This filter represents a first attempt by Meadowlark Optics to design and build a tunable birefringent filter. Like most prototype devices, the filter has experienced a number of mechanical and electrical problems that have required repair.

On inspecting the filter shortly after delivery, a flaw was noticed in the first filter element. Initially it appeared that one of the liquid crystal cells may have leaked. When the element was returned to Meadowlark, it was determined that the problem was actually cosmetic. The element was rebuilt to remove the flaw, which may have contributed to white light leakage, and the element was returned to NRaD.

Through the first quarter of calendar year 1993 the filter transmission and tuning characteristics were tested. The results of these tests were inconsistent and not always repeatable. After consultation with the engineers at Meadowlark, various tests of the filter elements independent of the computer drive electronics were performed. Based on these tests, the problem was isolated and determined to be in the driver card used to control the filter. This card was returned to Meadowlark for repair in April 1993.

In the process of evaluating the driver card, the engineers at Meadowlark found an error in the software used to drive the filter. This error was not detected before shipment because it was machine dependent (i.e., the software worked fine on some computers and not on others). After modifying the software, the driver board was tested and proved to be undamaged and working properly. The driver board and new software were returned to NRaD in May 1993.

While the driver board was being tested at Meadowlark, engineers at NRaD replaced the connector on element #6 that is used to monitor the temperature sensor. The connector that was originally installed broke shortly after the filter arrived, and attempts to replace the connector with one of the same type proved futile. The connector was replaced with a common 2.5-millimeter stereo phonograph plug.

In late July 1993, after extensive successful testing, the filter began to display transmission characteristics that were inconsistent with expectations. After testing the elements individually, it was determined that the second filter element (#2) had failed. The symptoms of the failure were that the transmission function showed twice as many peaks as expected, and interference fringes were evident across the face of the filter. This element was returned for repair in late July 1993.

Engineers at Meadowlark evaluated the element and determined that there were in fact two problems. A lead had broken on one of the liquid crystal variable retarders, accounting for the odd transmission characteristics, and the glue that held one of the triacetate layers on had begun to fail and separate, producing the interference fringes. Both problems were repaired and the filter returned to NRaD in early August 1993.

During discussions with the Meadowlark engineers about the problems that had developed in element #2, they indicated that they had been experiencing problems with the cement originally used, and that other elements might begin to experience lamination problems. Upon careful examination of the other elements, it was found that elements #4 and #5 were experiencing similar delamination problems. These elements were returned to Meadowlark for repair in the first week of August.

Upon receiving the decaying elements, Meadowlark estimated that element #6 could be repaired in about a week, but because of the complexity of element #4, it would require up to a month to repair. The delamination problem in element #4 had just begun at the edge of the component, and though it might eventually cover the entire element, at the time it still had not affected the clear aperture. Because the end of the fiscal year was approaching, and testing of the filter was not complete, the decision was made not to repair element #4. After repairs were completed on element #6, both elements were returned to NRaD in late August.

The filter elements have continued to decay with time. As of late November 1993 when this report was being completed, problems had developed in four of the elements. Element #2 shows the worst signs of delamination, with interference fringes over a full 30% of the aperture. This occurred in spite of the repairs that were performed on this element in July. Element #3 is showing signs of delamination in two separate and distinct locations involving different layers within the element. Element #4 is still showing fringes radiating out from one of the screw holes in the frame; however, the fringes do not seem significantly worse than they were in early August. Finally, element #5 is now showing symptoms almost identical to element #4. The only elements not showing signs of degradation at this time are elements #1 and #6.

UNCLASSIFIED

21a NAME OF RESPONSIBLE INDIVIDUAL G. L. Adams	21b TELEPHONE (include Area Code) (619) 553-3716	21c OFFICE SYMBOL Code 843

INITIAL DISTRIBUTION

Code 0012	Patent Counsel	(1)
Code 0274	Library	(2)
Code 0275	Archive/Stock	(6)
Code 80	K. D. Regan	(1)
Code 84	C. E. Gibbens	(1)
Code 843	D. M. Gookin	(1)
Code 843	G. L. Adams	(10)

Defense Technical Information Center
Alexandria, VA 22304-6145 (4)

NCCOSC Washington Liaison Office
Washington, DC 20363-5100

Center for Naval Analyses
Alexandria, VA 22302-0268

Navy Acquisition, Research and Development
Information Center (NARDIC)
Arlington, VA 22244-5114

GIDEP Operations Center
Corona, CA 91718-8000